1973-06

Fiber optic and laser digital pressure transducers.

Leonard, John Wallis

Monterey, California. Naval Postgraduate School

FIBER OPTIC AND LASER DIGITAL PRESSURE TRANSDUCERS

John Wallis Leonard

NAVAL POSTGRADUATE SCHOOL
Monterey, California

THESIS

FIBER OPTIC AND LASER DIGITAL
PRESSURE TRANSDUCERS

by

John Wallis Leonard

Thesis Advisor: A. E. Fuhs

June 1973

Fiber Optic and Laser Digital Pressure Transducers

by

John Wallis Leonard
Lieutenant, United States Navy
B.S., United States Naval Academy, 1967

Submitted in partial fulfillment of the
requirements for the degree of

MASTER OF SCIENCE IN AERONAUTICAL ENGINEERING

from the

NAVAL POSTGRADUATE SCHOOL
June 1973

ABSTRACT

The theory and response of fiber optic pressure transducers were investigated in a continuation of previous research. A 0.125 inch diameter transducer was built and statically tested. A probe consisting of two concentric glass fiber bundles was used to transmit light to and from the transducer diaphragm. Response was linear through 60 inches Hg. Linearity and sensitivity of response were dependent on diaphragm thickness and probe location, respectively. In a separate experiment, a gas laser was externally modulated by means of a moveable mirror. Axial movement of the mirror corresponding to half-wavelengths of laser radiation produced intensity maxima and minima. This modulation concept was extended to pressure measurement by attaching the mirror to a pressure sensing diaphragm.

TABLE OF CONTENTS

LIST OF FIGURES

LIST OF SYMBOLS

Fiber Optic Pressure Transducer:

a	diaphragm radius
D	initial probe displacement from diaphragm
E	Young's modulus
F	light flux
h	fiber diameter
I	light ray intensity
I_o	light ray intensity at fiber axis
L	fiber length
m	slope of triangular intensity distribution
n_o	index of refraction (external medium)
n_1	index of refraction (fiber)
n_2	index of refraction (fiber cladding)
N.A.	numerical aperture
p	pressure
R	radius on the diaphragm surface
r_o	inner fiber bundle radius
r_1	inner limiting radius
r_2	outer limiting radius
T	fiber transmission factor
t	diaphragm thickness
X	distance from diaphragm to probe
x	diaphragm deflection
x_{max}	maximum diaphragm deflection

x'	diaphragm slope
Y	point on probe face where reflected ray re-enters
θ	angle relative to fiber axis
θ_I	angle of incidence
θ_R	angle of refraction
θ_{crit}	critical angle for total internal reflection
ν	Poisson's ratio

Laser Digital Pressure Transducer:

A_R	amplitude of right running laser cavity wave
A_L	amplitude of left running laser cavity wave
A_o	peak amplitude of cavity wave
C_R	amplitude of right running external wave
C_L	amplitude of left running external wave
C_o	peak amplitude of external wave
f	fractional wavelength of mirror movement
L	location of external mirror from laser cavity
m	integer
n	number of half-wavelengths
t	time
x	axial distance
ϕ	phase angle
ω	radiation frequency
λ	radiation wavelength

ACKNOWLEDGEMENT

The author wishes to express his deepest gratitude to Professor Allen E. Fuhs for his assistance, guidance and time; to Naval Postgraduate School technician Mr. Bertis H. Funk for his invaluable technical services; and to Doctor Gilbert Hollingsworth of the Naval Air Development Center and Professor S. H. Kalmbach of the Department of Physics for providing equipment used in this research.

I. INTRODUCTION

Very small pressure transducers find many applications in flow measurement, notably in the testing of axial flow compressors. For this application, arrays of many such transducers are required. Two main types of transducer are in current use: semiconductor strain gage and piezoelectric, both having a typical diameter of from 0.05 to 0.25 inch. Continuing efforts are underway to reduce the size of these transducers, regardless of type.

Both piezoelectric and strain gage transducers have limitations that restrict their usage. Each employs internal sensing elements that are highly temperature sensitive. Strain gage transducers are limited by the natural frequencies of their sensing elements. Very small transducers also tend to be very expensive, costing up to $900.00 per unit.

This paper considers two new types of pressure transducers: fiber optic and laser digital. Accordingly, the research is presented in two major segments. The segment covering the fiber optic pressure transducer is a continuation of previous research, with the specific objectives of further miniaturization of the transducer and identification of parameters affecting its response. The segment covering the laser digital pressure transducer is an investigation into an entirely new concept of pressure measurement, derived from laser interferometry.

II. FIBER OPTIC PRESSURE TRANSDUCER

A. DEFINITIONS

Before beginning this section, it is necessary to define some frequently used terms pertaining to basic fiber optics and, in particular, the fiber optic pressure transducer:

1. Diaphragm: A thin, circular plate mounted on the pressure sensing end of the transducer.
2. Fiber Bundle: A grouping of many optical fibers.
3. Probe: An arrangement of transmitting and receiving fiber bundles which is inserted into the transducer. Refer to Figure 1a.
4. Transducer: A hollow metal cylinder, one end of which supports the diaphragm.
5. Fiber Optic Pressure Transducer: Diaphragm, transducer, probe, and fiber bundles assembled as a unit. Refer to Figure 1b.

B. CONCEPT

The fiber optic pressure transducer uses two flexible fiber bundles for transmitting light to and from the surface of a pressure sensing diaphragm. At the transducer end, the fiber bundles form a probe which is inserted into the transducer. At the opposite end, the two fiber bundles separate into a Y-configuration. The inner fiber bundle is connected to a light source and the outer fiber bundle is connected to a photomultiplier tube. Refer to Figure 1.

As pressure is applied to the transducer, the diaphragm deflects and bows inward. This produces a change in the amount of light flux reflected from the diaphragm into the outer fiber bundle. The change in light flux is detected at the photomultiplier tube and displayed on a photometer.

The typical fiber optic pressure transducer employed in this research appears in Figure 1. This concept has several inherent advantages. The flexible fiber bundles can be made in lengths of three feet or more, depending on light source intensity and optical quality of the fibers. High temperature applications are possible when the fiber bundles are encased in a flexible metal sheath. Optical fibers made of glass have an operational temperature range of up to 1000 degrees Fahrenheit; this range is within the limits of axial compressor operation. Fiber bundles are commercially available in diameters of 0.030 inch or smaller, depending on manufacturing expertise.

The light source and photomultiplier tube are located remotely from the transducer and as such are insensitive to the transducer environment. The frequency response is limited to that of the small, clamped diaphragm, rather than that of sensing elements within the transducer.

The concept also has several restrictions. At the probe face, the fiber bundles must be flat and optically polished for consistent response. The diaphragm must be uniformly and hermetically clamped to the transducer. The measurement of small changes in reflected light output requires a very

stable light source and photomultiplier tube. For dynamic pressure measurement, the photomultiplier tube and indicator must be capable of response to rapid changes in the reflected light output.

C. OPTICAL FIBER AS A LIGHT TRANSMITTING MEDIUM [Refs. 1-4]

Light is transmitted along transparent fibers of glass, plastic, or other similar media by the phenomenon of total internal reflection. A ray of light, incident upon the interface between two optically transparent materials having different indices of refraction, will undergo total internal reflection if:

1. the ray is incident upon the interface from the direction of the denser material; and
2. the angle made by the ray with the normal to the interface is greater than some critical angle. This angle is dependent on the indices of refraction of the materials.

Optical fibers consist of a cylindrical core material with index of refraction n_1 surrounded by a cladding material with index of refraction n_2. Light rays reflected along a fiber are classified as either meridional or skew. Meridional rays are those that intersect the fiber axis. Skew rays never intersect the fiber axis although their behavior resembles that of meridional rays in all other respects. Rigorous analysis of the geometric optics of skew rays can become complex; only their overall effect will be considered.

Total internal reflection of a meridional ray occurs at the core-cladding interface when the angle of the ray measured with respect to the fiber axis is less than a critical angle, θ_{crit}, given by:

$$\theta_{crit} = \sin^{-1} \left[(n_1^2 - n_2^2)^{\frac{1}{2}} / n_1 \right]$$

Light from an external source incident upon the face of an optical fiber will be either reflected from the face or refracted and transmitted through the fiber, depending on the angle of incidence and the indices of refraction of the core and external medium. The relation between angle of incidence, θ_I, and angle of refraction, θ_R, is expressed by Snell's Law as

$$n_o \sin \theta_I = n_1 \sin \theta_R$$

where n_o = external medium index of refraction ($n_{o_{air}} = 1$).

A basic descriptive characteristic for any optical fiber is numerical aperture, which represents the size of the light acceptance cone and is mathematically expressed as the sine of the half-angle of the acceptance cone θ_{max}. From Snell's Law,

$$\text{N.A.} = \sin \theta_{max} = (n_1^2 - n_2^2)^{\frac{1}{2}} / n_o \ .$$

Refer to Figure 2.

From a purely geometric standpoint, light is transmitted along an optical fiber at a constant angle with the fiber axis. Deviations from the true path occur, however, from imperfections in the fiber and core-clad interface, and

surface scattering upon entry. Internal scattering is proportional to fiber length; therefore, longer fibers must be of higher optical quality for useful light transmission. Surface scattering occurs readily when there are irregularities in the face of the fiber; scratches and pits in the face diffuse light rapidly.

The emergent cone angle is actually wider than predicted by geometric optics. Skew rays, striae, and face imperfections have the effect of expanding and distorting the emergent cone. Bending the fiber tends to reduce the transmission efficiency.

The light intensity distribution for emergent rays is given by Morita, Reference 4, as a function of the angle, θ, with respect to the normal to the face of the fiber:

$$I = I_o T^2 \alpha^{(L/2h)\tan\theta - \beta L \sec\theta}$$

where L and h are length and diameter, respectively, and α and β are constants related to optical quality. A representative distribution appears in Figure 3.

Up to this point the discussion has dealt only with single optical fibers. When many optical fibers are grouped into a fiber bundle, light leakage, known as crosstalk, can occur between adjacent fibers. This phenomenon occurs as a result of evanescent waves near a fiber surface being trapped and transmitted by adjacent fibers or along the interstices between fibers. The amount of light leakage from a fiber surface is a measure of optical quality. For

total elimination of crosstalk, optical fibers must be fabricated with numerical aperture of one or greater, or coated with a second highly absorbing or reflecting material [Ref. 5].

D. PROBE AND FIBER BUNDLE DESIGN

Recalling that the transmission loss in an optical fiber is a function of fiber length and end losses, it follows that the amount of light flux emerging from the outer fiber bundle always will be less than the original light flux entering the inner fiber bundle. Irrespective of size or quantity of fibers, transmission efficiency of a fiber bundle is approximately 50% for a six-foot length, and 20% for a twelve-foot length. Since the photomultiplier tube measures an output produced by passing light in two directions, the measured output represents a small fraction of the original input from the light source. While length and flexibility are desirable, the fiber bundle must be of a length that insures an output compatible with the sensitivity of the measuring device.

The probes and related fiber bundles used in this research incorporated flint glass optical fibers, of diameter 3 mils and numerical aperture of 0.56 (1 mil = 0.001 inch). Two probe fiber bundle combinations were used, each employing a concentric arrangement of transmitting and receiving fiber bundles. The larger, manufactured by MTI, Incorporated, had a probe 3.0 inches in length and flexible fiber bundles 36.0 inches in length. The probe was

encased in a metal sleeve 0.108 inch in diameter, and the fiber bundles were surrounded by rubber tubing. For this probe, outer fiber bundle diameter was 0.10 inch, and inner inner fiber bundle diameter was 0.05 inch. A smaller probe-fiber bundle combination was manufactured within the Aeronautics Department. The probe and flexible fiber bundles were 2.5 inches and 8.0 inches long, respectively, and surrounded by rubber tubing 0.090 inch in diameter. The outer fiber bundle was 0.080 inch in diameter, and the inner fiber bundle was 0.040 inch in diameter.

E. DIAPHRAGM AND TRANSDUCER DESIGN

Analysis of the deflection and curvature of a circular plate with a clamped edge condition is covered in Appendix A. Using Equation (A-2) for the maximum deflection, design curves for stainless steel diaphragms of several representative dimensions were obtained (Figure 4).

Two stainless steel diaphragms were used for the majority of the research. The smaller diaphragm, associated with the smaller transducer and probe, was 1.0 mil thick and had a diameter of 0.090 inch. The larger diaphragm, tested with the MTI probe, was 1.5 mils thick, with a diameter of 0.110 inch.

The diaphragms were silver soldered to the transducers. This method insured a hermetic seal and approximated the clamped edge condition assumed in Appendix A but was somewhat less than optimal. Close examination of the transducers revealed that small amounts of resin from the solder had

collected on the inner reflecting surfaces of the diaphragms, despite application of cleaning solvent to the transducer interiors. Also, small amounts of solder were visible at points on the transducer-diaphragm interface; therefore, the clamped edge condition was not perfectly uniform. A more ideal method of mounting would employ a separate collar-like device to clamp the diaphragm to the transducer. This method, however, would require very close tolerances to maintain a strong, hermetic seal at higher pressures and would increase the overall size of the transducer.

F. DISPLACEMENT MEASUREMENT WITH A PROBE [Ref. 6]

In recent years, fiber optics have been employed in a number of remote measuring techniques, notably in medical and quality control applications. The displacement measurement technique is accomplished with the use of adjacent groupings of transmitting and receiving fibers. The displacement of the working surface relative to the fibers is measured by detecting the amount of light reflected from the surface as in Figure 5. The probe manufactured by MTI, Incorporated, was intended for this application.

When the probe is in contact with the working surface, no light is reflected to the outer fiber bundle. As the distance between the probe and working surface increases, the cone of emergent light from the inner fiber bundle illuminates an increasingly larger area on the working surface. A secondary cone of light is reflected from this area to an increasingly larger portion of the outer fiber

bundle. The output light flux measured by the photomultiplier tube increases with displacement in a linear fashion until a peak output is reached, after which decreasing output is observed with increasing displacement.

The relationship between light output and working surface displacement (hereafter referred to as the displacement curve) can be divided into three regions, as shown in Figure 5. The near side, which is almost linear, is very sensitive to displacement. The peak of the displacement curve occurs at the displacement for which the outer fiber bundle is first completely illuminated by reflected light. In the region near the peak, the slope of the displacement curve changes rapidly, and light output is no longer a linear function of displacement. On the far side of the curve, the outer fiber bundle remains fully illuminated, but increasing amounts of light are reflected from the working surface to points outside the outer fiber bundle. Here it must be pointed out, however, that the effect of a reflecting wall that surrounds the probe and working surface has not yet been considered.

The reflectivity of the working surface has a distinct effect on the shape of the displacement curve. The general shape of the curve remains the same, and the peak always occurs at the same displacement; but reflectivity of the working surface is manifested in vertical shifts of the curve. For a working surface that is mirror-like, one observes a steep displacement curve. For a surface that

has low reflectivity, one observes a curve that is much flatter in comparison. Comparing displacement curves for different surfaces measured with the same probe, a downward shift in the curve is observed as reflectivity of the working surface decreases, as shown in Figure 6.

Thus far, the discussion has avoided the effects of secondary reflective surfaces other than the working surface itself. When the probe and working surface are surrounded by a tube, as in a transducer, the displacement curve is modified somewhat. The near-side light output remains the same, but light output on the far side is increased due to wall reflections. Appendix B presents an analysis of wall reflection, and the effect on the displacement curve is illustrated in Figure 7.

The probe manufactured by MTI, Incorporated, was used to obtain a displacement curve. The experimental curve is compared with that obtained from theory in Figure 8.

G. DIAPHRAGM DEFLECTION MEASURED WITH A PROBE

Probes used in the displacement measurement application have a typical operating range of one inch to ten microinches. The diaphragms used in this research experience a maximum centerline deflection of 500 to 700 microinches at a pressure of 100 inches Hg. Disregarding the effects of curvature and wall reflections, these displacements are measurable in principle. Measurement of very small displacements is a function of photomultiplier tube sensitivity and light source stability.

Considering the characteristic displacement curve of Figure 5, a probe initially positioned on the near side of the displacement curve relative to the diaphragm should produce a light output that decreases with increasing pressure. A probe positioned at the peak should produce a negligible output for the small deflections of the diaphragm, and a probe positioned on the far side should produce increasing output with increasing pressure. The experimental results were to the contrary, however.

Curvature of the diaphragm and wall reflections produce a variation from the case of the flat reflecting surface. From geometric optics, curvature would produce a wider reflected cone of light from the diaphragm than from a flat surface. The wider cone for a given deflection would produce a more sensitive pressure response (in terms of light output) when the probe is on the near side and a less sensitive response when the probe is on the far side. Wall reflections, from Figure 7, extend the range of the probe at large distances from the diaphragm, as the light output on the far side is increased.

In Reference 7, the pressure response of several different probe geometries at both near and far side positioning of the probe was investigated. A consistent response was observed - for all probe geometry and position combinations, the light output decreased as pressure was increased. The same characteristic response was observed in the present research. In addition, decreasing light output with

increasing pressure was observed with the probe positioned at the peak of the displacement curve and up to 0.750 inch away from the diaphragm.

H. OPTICAL COUPLING THEORY

An analytic theory of optical coupling between the probe and a reflecting surface was developed to numerically predict the reflected light output for given shapes of the surface and its location relative to the probe. For this discussion, "reflecting surface" applies to both flat surfaces and curved diaphragms. The theory was applied to both cases.

The geometric analysis of light reflection from the inner fiber bundle to the outer via the reflecting surface is developed in Appendix C. The inner and outer fiber bundles are treated as two homogeneous optical fibers rather than as bundles consisting of many fibers. Figure 9 illustrates the geometry of light reflection. The analysis results in the determination of two limiting radii, r_1 and r_2, on the face of the inner fiber bundle. The region within the limiting radii represents the portion of the emergent light cone that is received in the outer fiber bundle via the reflecting surface. The region varies in size, radial location, and intensity as a function of surface location, curvature, and combinations thereof.

In calculating the light flux in the fractional part of the cone bordered by the limiting radii, it is necessary to consider the non-uniform light intensity across the face of

the inner fiber bundle. To facilitate integration, a triangular light intensity distribution was assumed (Figure 3). With this assumption, the light intensity, I(r), at a radius, r, is

$$I(r) = \frac{r_o - r}{m} \qquad (1)$$

where m is the slope of the triangle and r_o is the inner fiber bundle radius.

The intensity attenuation as a function of axial distance from the probe face also must be considered. Intensity measured at a distance, d, from the face of the probe is

$$I_d = \frac{I_o}{(1 + \frac{d}{Z})^2}$$

where $Z = r_o \cot\theta_R$. The slope of the triangular intensity distribution is then

$$m = - \frac{r_o}{I_d} .$$

Applying this result to Equation (1),

$$I(r) = I_d \left(\frac{r_o - r}{r_o}\right) .$$

The light flux, F, reflected from the surface to the outer fiber bundle is

$$F = 2\pi \int_{r_1}^{r_2} I(r) r dr$$

$$F = 2\pi \left[\frac{r_o r^2}{2m} - \frac{r^3}{3m}\right]_{r_1}^{r_2} .$$

In applying the theory to displacement measurement from a flat surface, as described in Section F, the pressure is held constant at zero, and the light output becomes a function of probe-surface displacement (refer to Appendix C). Figure 8 compares the experimental displacement curve with that calculated from theory. In the case of the pressure transducer, light output becomes a function of diaphragm deflection, curvature, and wall reflection effects. From the experiments, diaphragm curvature is dominant but is not adequately handled by simple geometrics. The wall reflection effects are not included in the model, and changes in light output were observed, with the probe at distances (up to 0.750 inch) from the diaphragm, that greatly exceeded the geometric limits of the model. Calculated light output curves appear as a matter of general interest in Figure 10, although the predicted trends do not agree with the observed trends.

I. EXPERIMENTAL EQUIPMENT

A typical arrangement for the pressure tests appears in Figure 11a, and a picture of the equipment appears in Figure 11b. Pressure to the test chamber was supplied from a Lockheed mobile pressure test rig and monitored on a Wallace and Tiernan pressure gage. The gage was accurate to ±0.50 inch Hg. For the displacement measurement tests, the transducer and pressure chamber were replaced by a calibration device consisting of a flat, reflecting, non-rotating surface that was moved axially by turning a micrometer dial.

First attempts at testing the transducers and probes required some experimentation with light sources. A General Electric 55x instrument bulb, rated at 7 volts and 0.41 ampere and connected through a small transformer to the AC wall outlet, was first employed. This light source was much too unstable to provide a useable output, although trends in light output were observable.

A Hughes model 1710 He-Ne laser, rated at 10 milliwatts, was next employed. This arrangement was more stable than the previous one and yielded marginally useable output. Use of the laser as a light source presented some serious drawbacks, however. The power output of the laser was considerably more than required for the application and led to restrictions on photometer gain and sensitivity settings. Also, alignment of the laser beam with the end of the inner fiber bundle had a marked effect on the size and intensity of the emergent light cone at the probe face. Placement of one's hand on the equipment bench produced changes in light output from the disturbed alignment. Due to the extreme alignment sensitivity, lasers are not recommended as direct light sources. Plots of light output versus pressure using the laser light source appear in Figure 12.

The most stable light source arrangement incorporated the General Electric 55x bulb and a Sorensen DC power supply. All experimental results, except Figure 12, were obtained with this light source arrangement.

J. DESCRIPTION OF TESTS

1. Displacement Measurement

The probe manufactured by MTI, Incorporated, was used to obtain an experimental displacement curve for comparison with theory. The inner and outer fiber bundles were connected to the light source and photomultiplier tube, respectively. The probe was mounted in the micrometer device. With the probe and reflecting surface initially in contact, the surface was moved away from the probe in uniform increments by rotating the micrometer dial. Light output was measured at the photometer for 0.005 inch increments out to 0.080 inch. Comparison of the normalized output curve with theory appears in Figure 8.

2. Fiber Optic Pressure Transducer Response

For each of these tests the transducer was inserted in a small pressure chamber connected by a flexible air hose to the Lockheed pressure test rig. Pressure supplied from the rig was varied in 5.0 inch Hg increments, and light output was measured at the photometer.

The larger MTI probe and associated transducer with 1.5 mil diaphragm were used to investigate light output as a function of pressure and the initial probe to diaphragm displacement. For this test, the light output on the photometer was monitored on the photometer as the probe was moved away from the unpressurized diaphragm, until the peak light output was observed. With the location of the probe corresponding to the peak of the displacement curve thus

established as a reference, the tests were repeated for probe locations corresponding to the near side, peak, and far side of the displacement curve. Normalized light output versus pressure plots for both transducer-probe combinations appear in Figures 12-16.

3. Effect of Pressurized Diaphragm on Peak of Displacement Curve

The relationship of light output versus probe location from the diaphragm had the same characteristic form as the displacement curves of Figure 7, with the addition of the wall reflection effects. As an extension of the analysis presented in Appendix B, it was desirable to investigate the effect of the pressurized, curved diaphragm on the peak light output of the displacement curve. With the pressure on the diaphragm initially set at zero, the probe was moved within the transducer until the peak light output was observed on the photometer. The probe then was moved closer to the diaphragm, and pressure was applied. Moving the probe within the transducer again, the peak light output was observed on the photometer. This procedure was repeated in 20 inch Hg increments. The plot obtained appears in Figure 17.

4. Effect of Probe Position on Light Output

This test was performed as a means of measuring the range of light output over the full pressure range of 0 to 100 inches Hg, as a function of various stationary positions of the probe within the transducer. The probe was initially positioned 0.750 inch from the diaphragm. Light output was

then observed for 0 inches Hg and 100 inches Hg. The procedure was repeated as the probe was repositioned nearer the diaphragm. Light output range versus probe position is plotted in Figure 13.

K. TEST RESULTS AND DISCUSSION

1. Displacement Curve

The theoretical and experimental displacement curves are plotted in Figure 8. The curves agree qualitatively, and the near sides correlate reasonably well. The half-angle of the emergent light cone was measured to be approximately 27.0 degrees, and the inner fiber bundle radius was 0.025 inch. If both values, as used in the calculation, were slightly smaller, full illumination of the outer fiber bundle would be predicted at a greater displacement in closer agreement with experiment. In particular, the smaller the ratio of inner fiber bundle radius to the outer fiber bundle radius, the greater is the displacement at the peak. A smaller inner fiber bundle requires a greater displacement to fully illuminate the outer fiber bundle.

The experimental far side slope is much less than the theory predicts. Since the theory assumes a perfect reflecting surface, the calculated displacement curve is steep. The actual surface was comparatively dull, and a flatter experimental displacement curve was observed. The difference could also be due in part to the assumption of a triangular light intensity distribution.

2. Pressure Transducer Tests

From Figure 13, the response of the smaller, 0.125 inch diameter transducer is linear to 60 inches Hg. The deflection of the 1 mil thick diameter diaphragm exceeds one-half the thickness at 40 inches Hg. The light output decreases at a lesser rate as the deflection approaches the thickness. Figure 12 shows similar results observed with a laser light source. The same trend of decreasing light output with increasing pressure is shown in Figures 14-16, using the larger MTI probe and 1.5 mil thick diaphragm. For both the near and far side probe locations, the response is linear over nearly the entire pressure range. At 100 inches Hg, the deflection of the 1.5 mil diaphragm remains less than one-half the thickness. The far side response is more sensitive, as was also observed with the smaller transducer.

The optical coupling theory, when applied to the pressure transducer, did not predict the observed response trend. Although wall reflection effects are not considered in the theory, they do not affect the trend of decreasing light output. When the transducer is reversed in the pressure chamber, the same response is observed despite the absence of the transducer walls. The wall reflection effects contribute primarily to the observed response with the probe at large distances from the diaphragm. It is concluded that diaphragm curvature is the dominant factor in the decreasing light output.

It was not possible to precisely measure the displacement of the probe relative to the diaphragm to an accuracy greater than the deflection of the diaphragm. It is seen, however, that the range of light output is greatest when the probe is positioned near the peak of the displacement curve (Figure 18). Figure 17 indicates that pressurizing the diaphragm decreases the light output at the peak of the displacement curve. Recalling the surface reflectivity effects discussed in Section F, the peak light output, as measured with a flat surface, is only affected by the reflectivity of the surface and always occurs at the same displacement with the same probe. If it were possible to precisely measure the distance between probe and diaphragm, and the peak displacement was found to occur at the same axial displacement from the pressurized diaphragm, it could be deduced that the diaphragm curvature reduces the effective flat reflecting area as seen by the probe and produces an effect similar to reducing the overall reflectivity of the diaphragm. In this case the decreasing light output would represent the vertical shifts in the displacement curves of Figure 6.

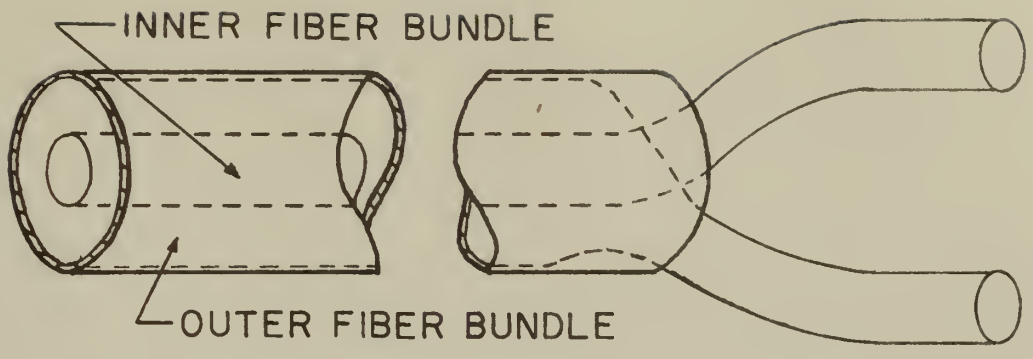

a) Detail of probe.

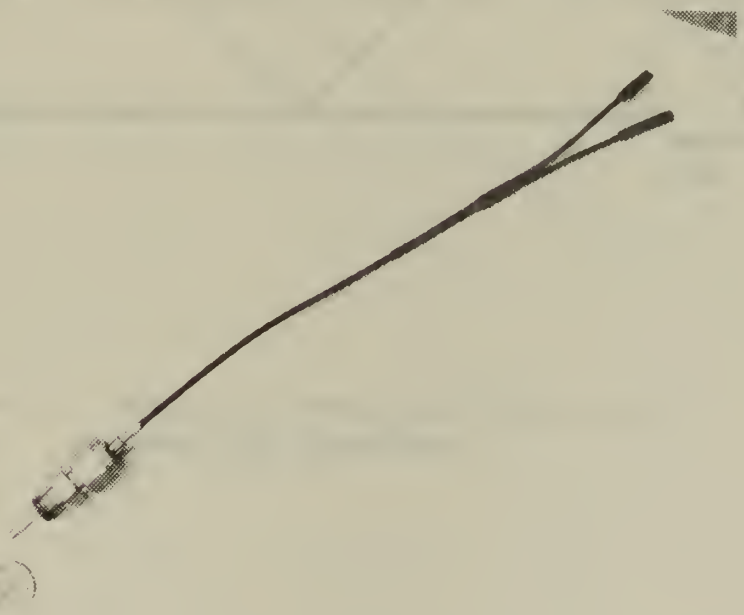

b) Fiber Optic Pressure Transducer.

Figure 1. Detail of Probe and Fiber Optic Pressure Transducer.

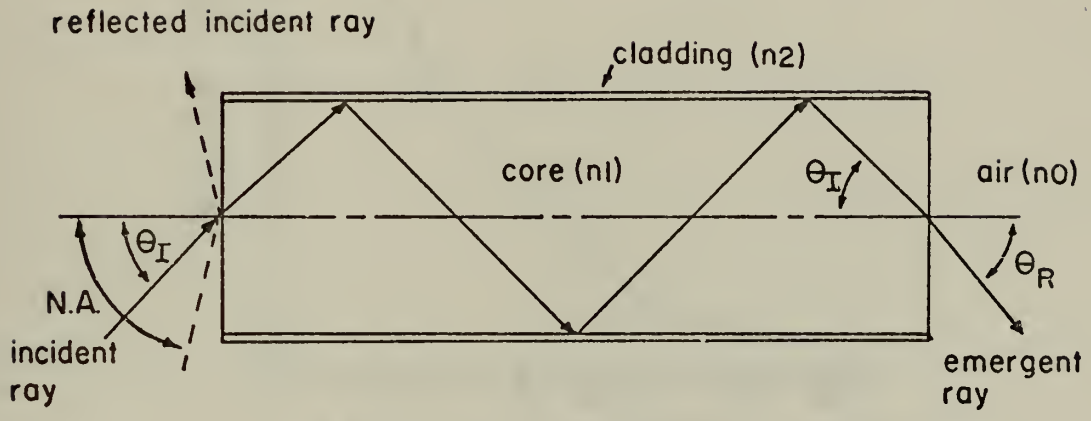

Figure 2. Total Internal Reflection and Numerical Aperture.

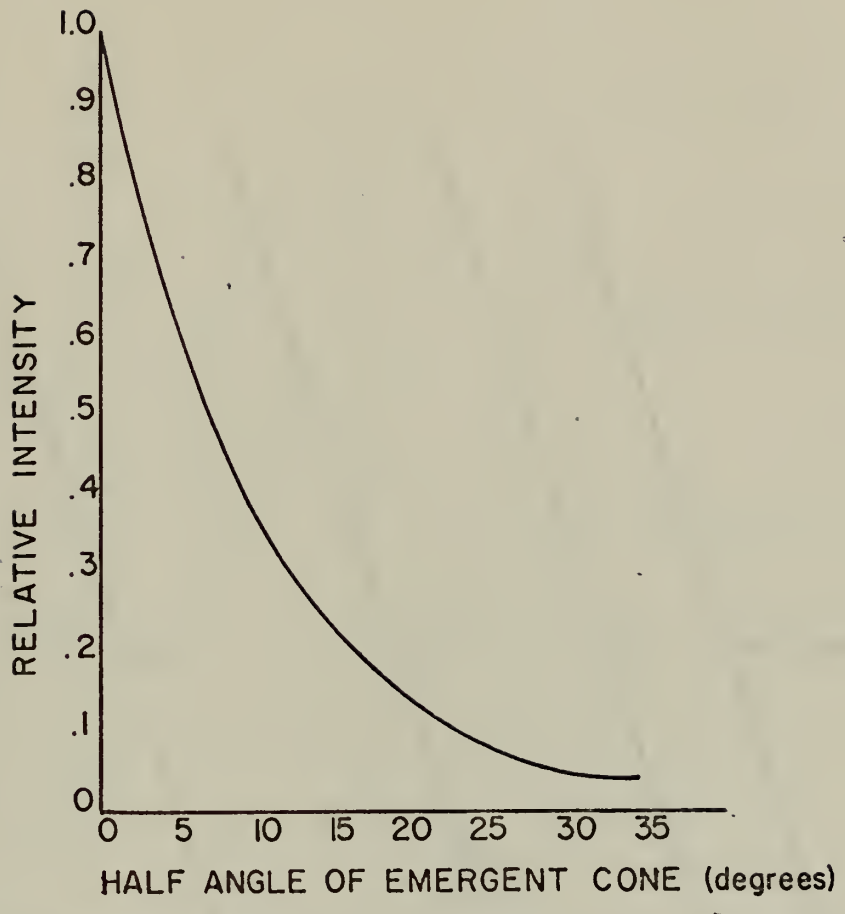

a) Angular intensity distribution, adapted from reference 4.

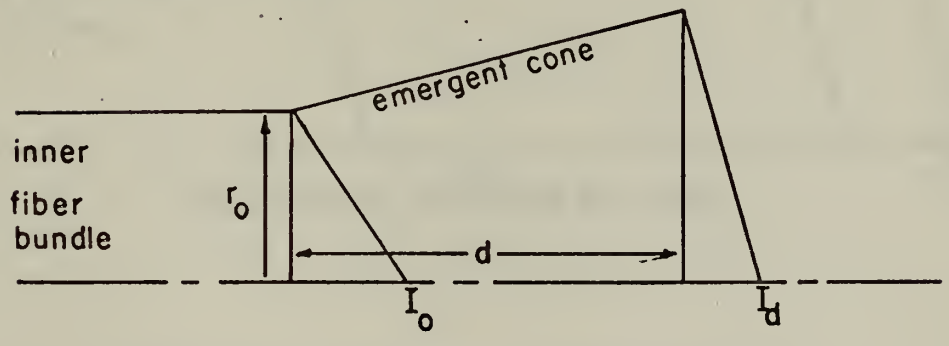

b) Triangular intensity distribution.

Figure 3. Light Intensity Distributions.

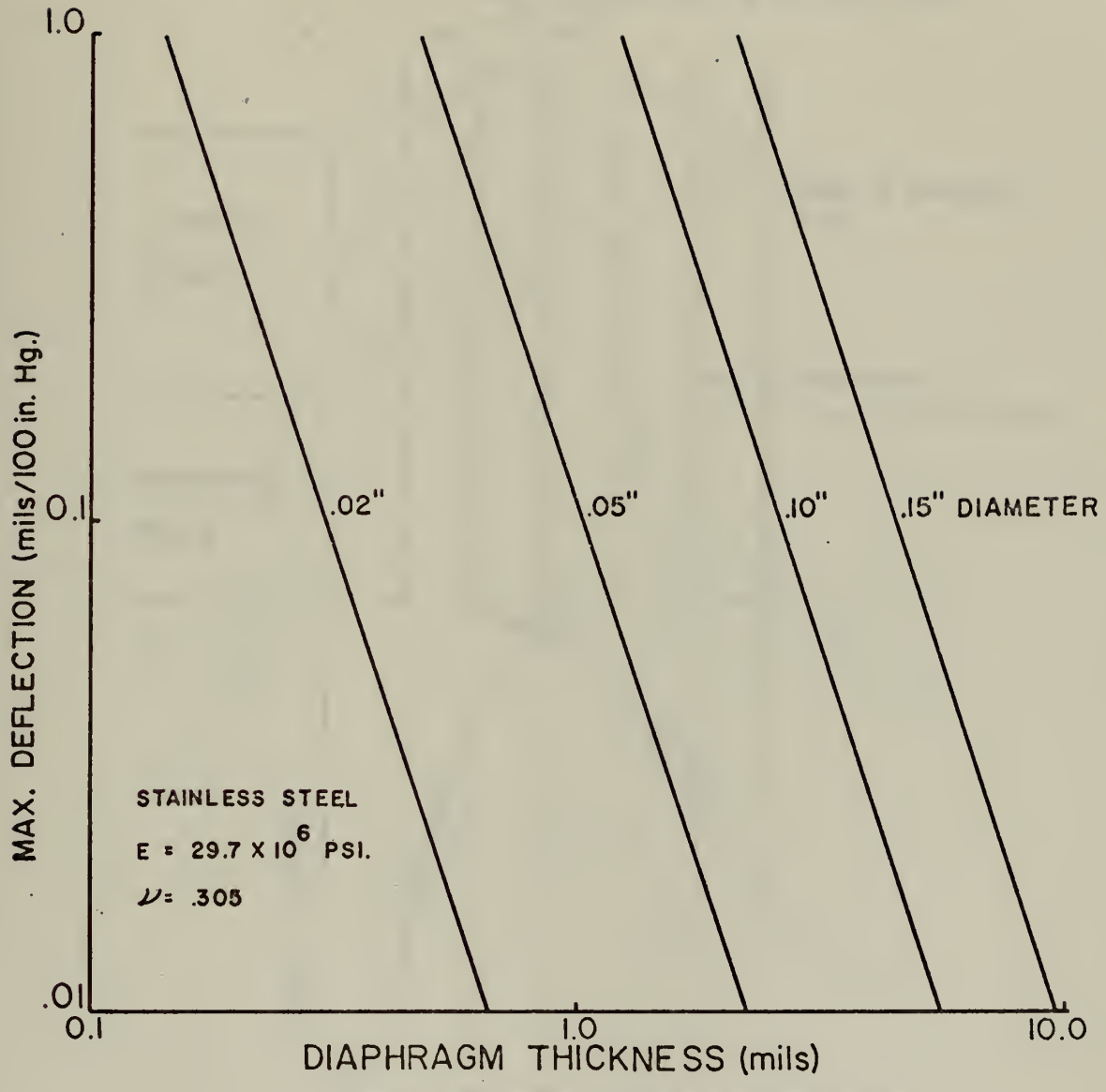

Figure 4. Diaphragm Design Curves.

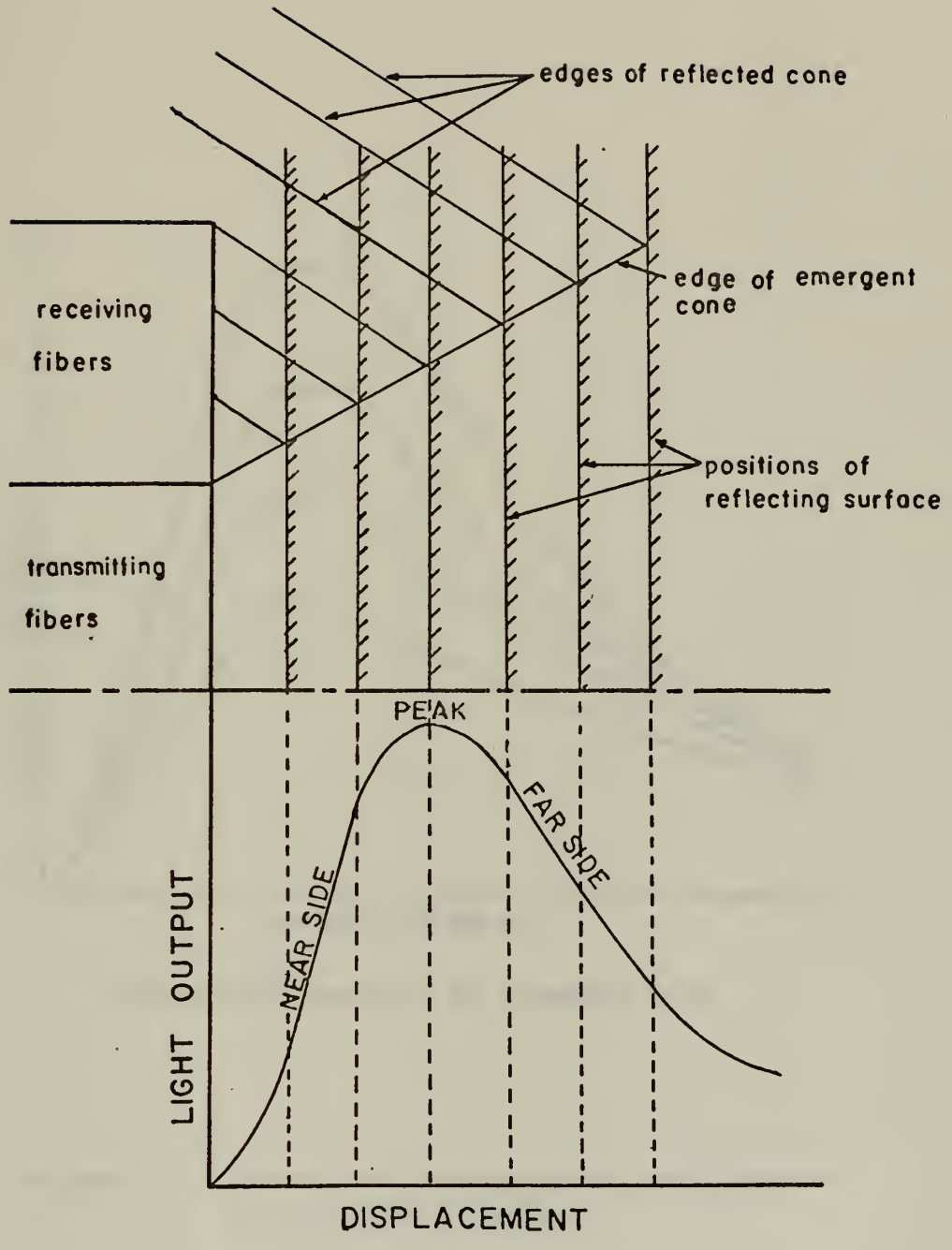

Figure 5. Principle of Displacement Measurement, adapted from Peference 6.

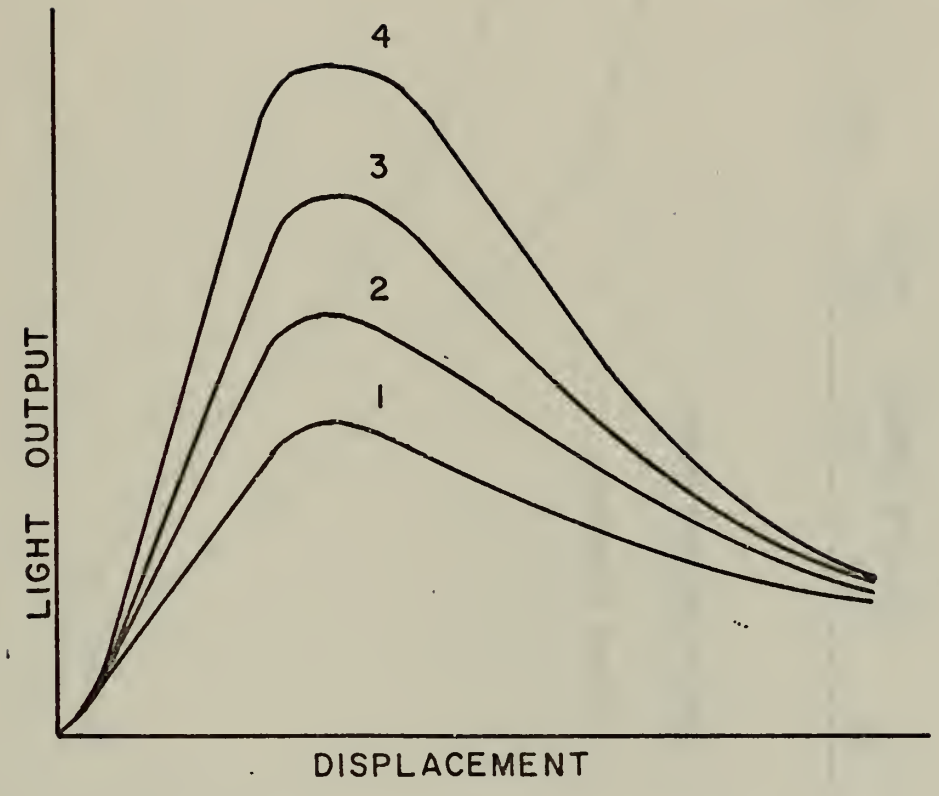

Figure 6. Effect of Surface Reflectivity on Displacement Curve.

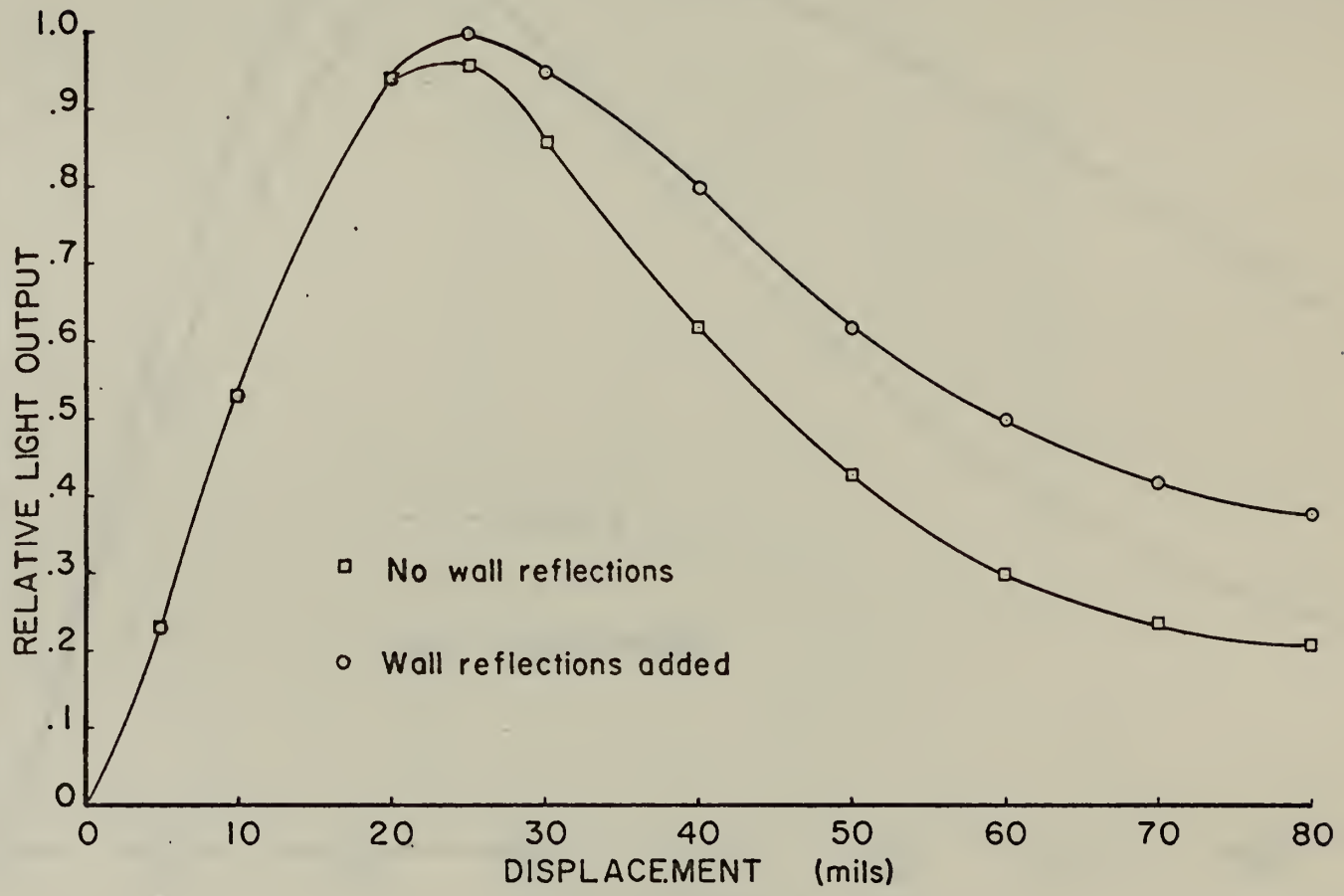

Figure 7. Wall Reflection Effect on Displacement Curve.

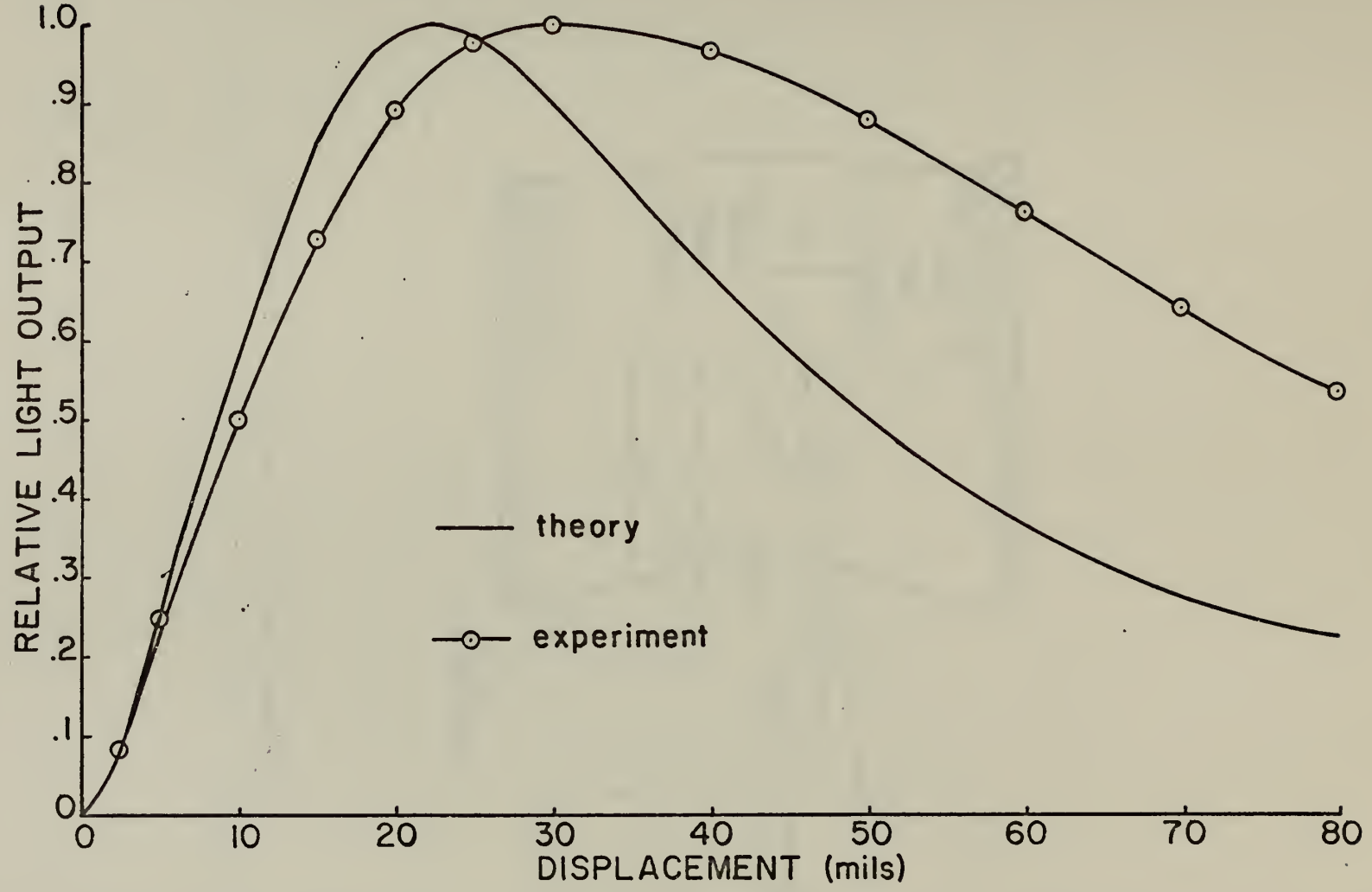

Figure 8. Theoretical and Experimental Displacement Curves.

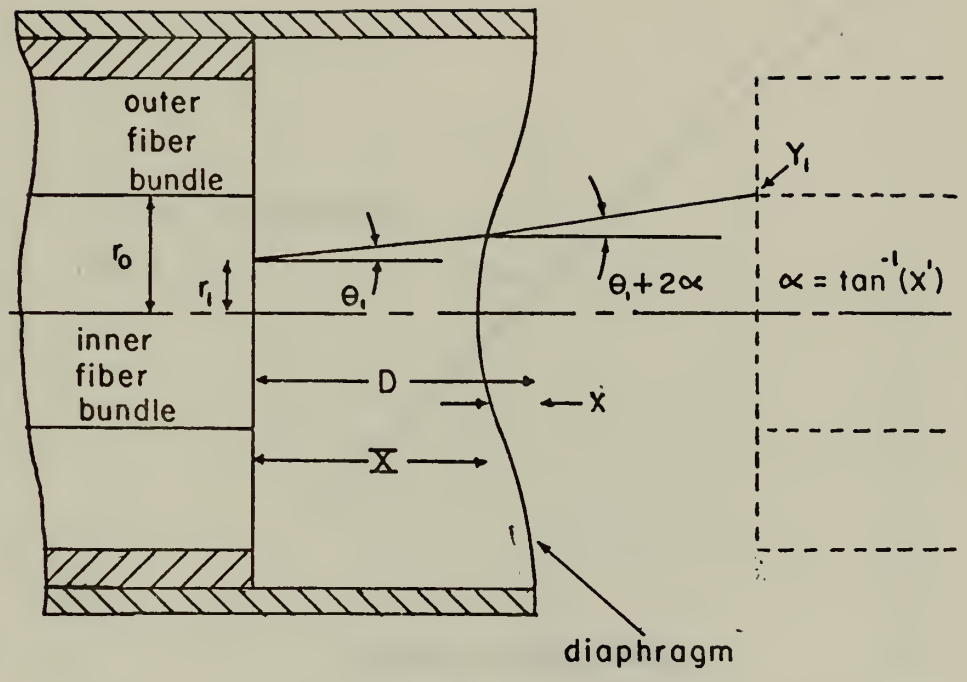

Figure 9. Optical Coupling Geometry.

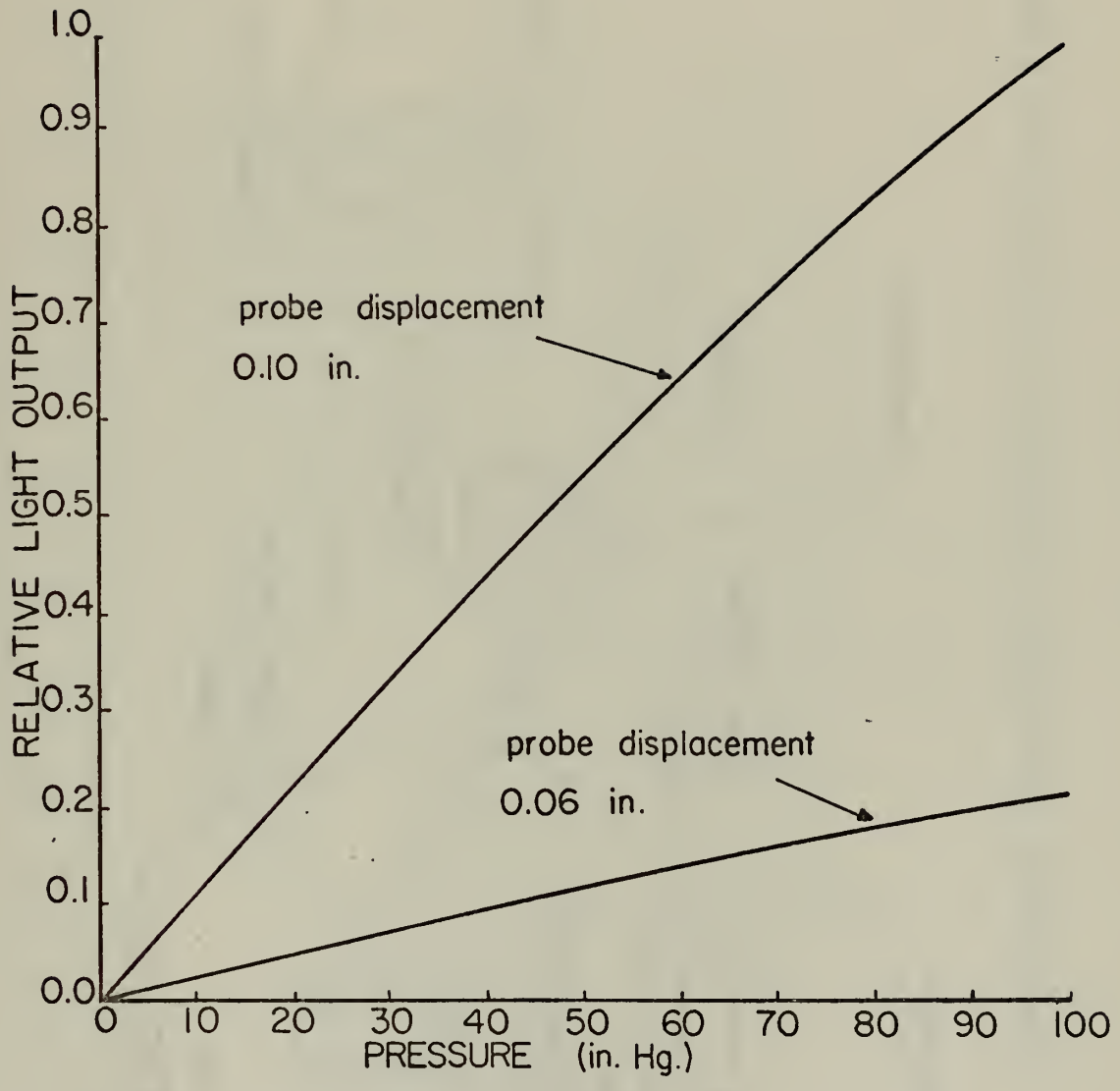

Figure 10. Calculated Pressure Transducer Response.

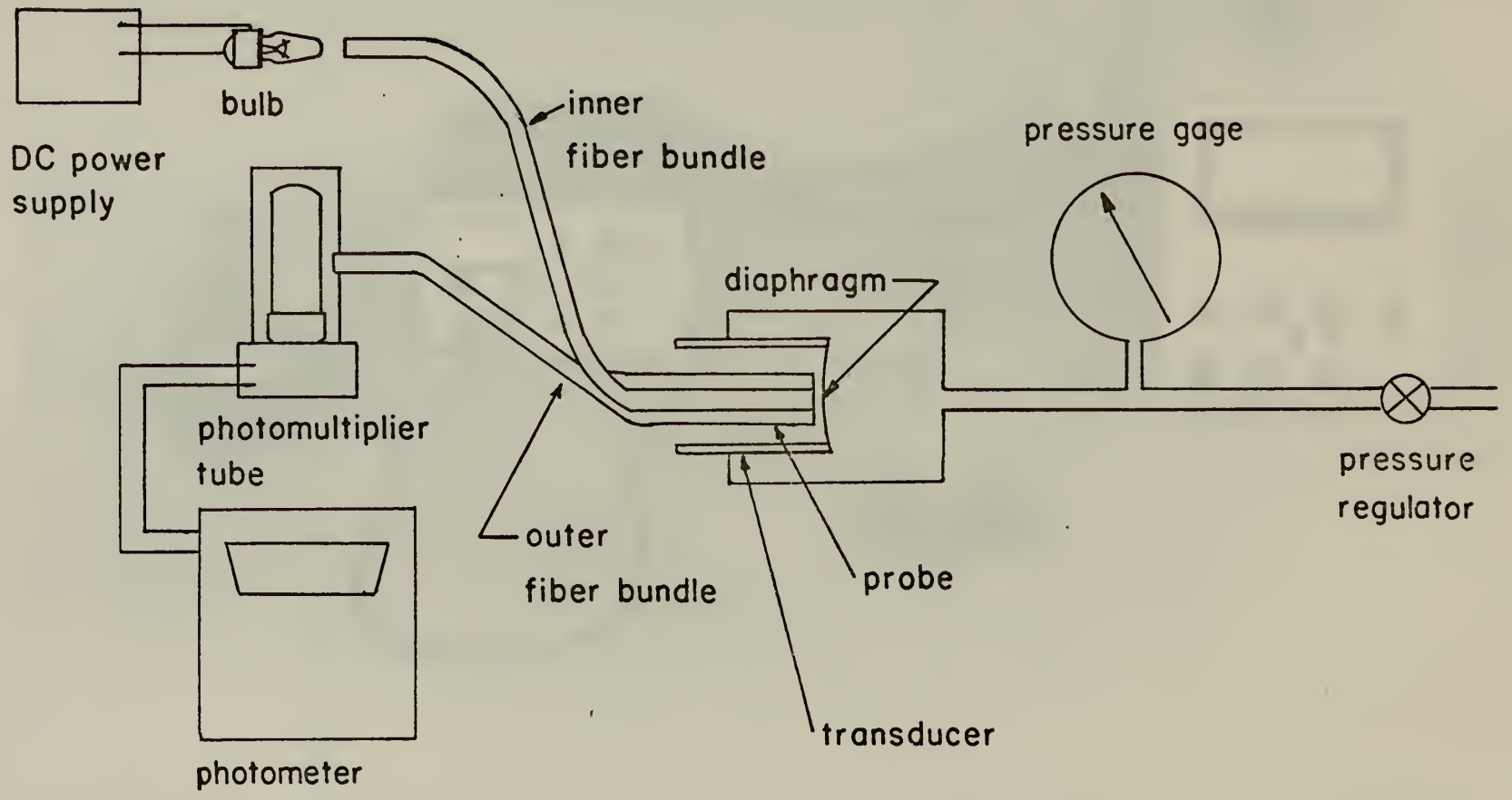

Figure IIa. Experimental Arrangement for Testing of Fiber Optic Pressure Transducer.

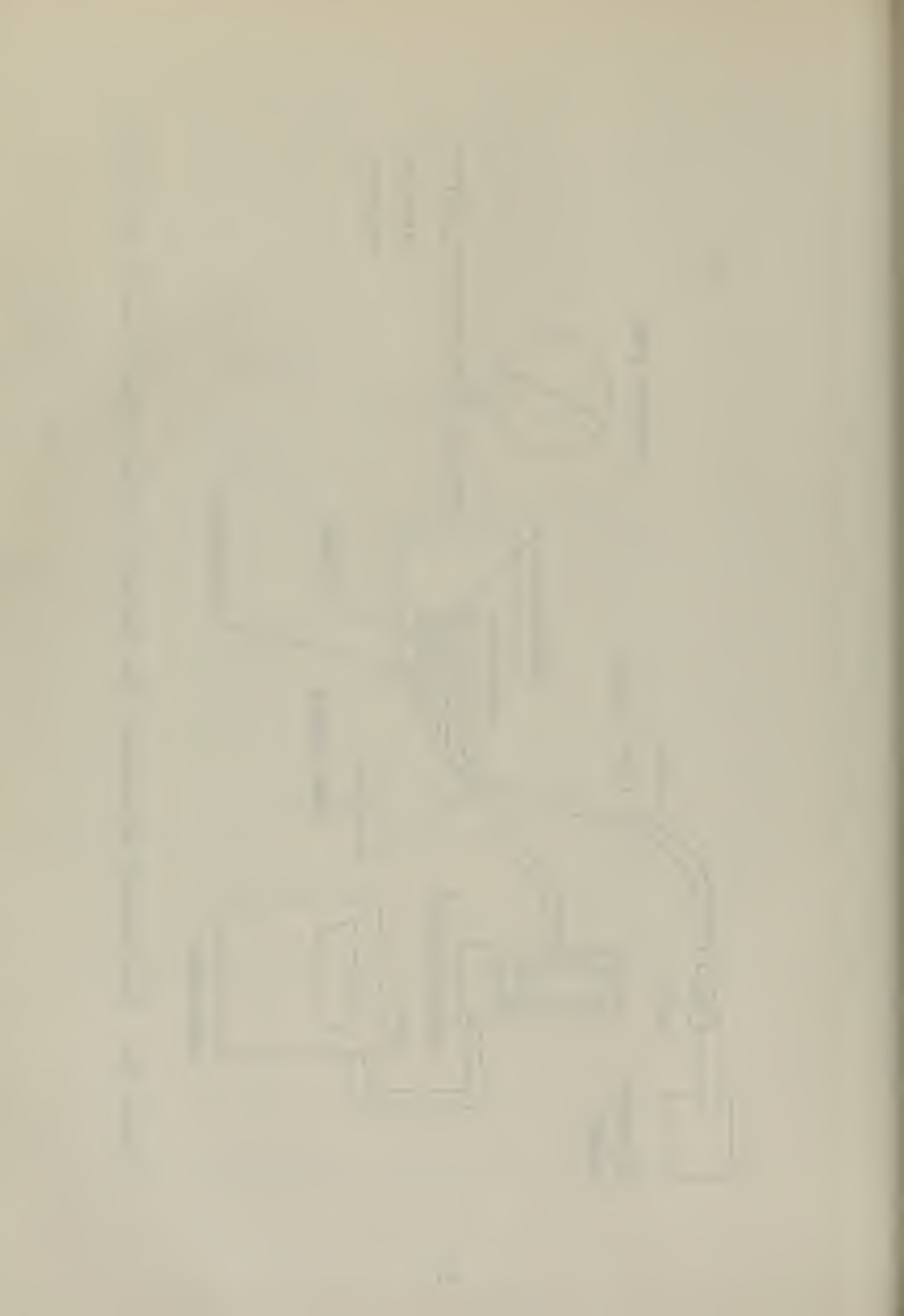

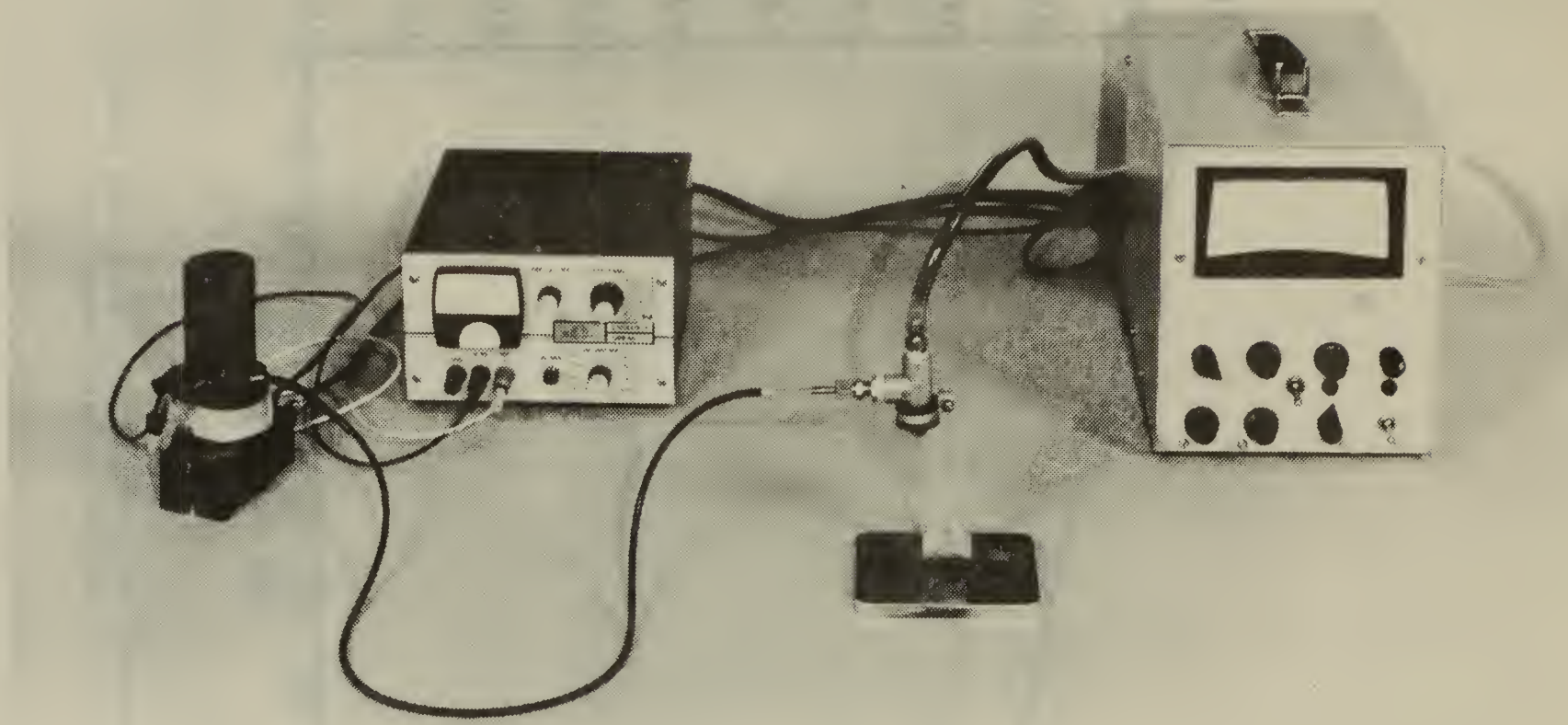

Figure 11b. Experimental Arrangement for Testing of Fiber Optic Pressure Transducer. Components from left are: light source and photomultiplier tube, DC power supply, fiber optic pressure transducer, pressure chamber, and photometer.

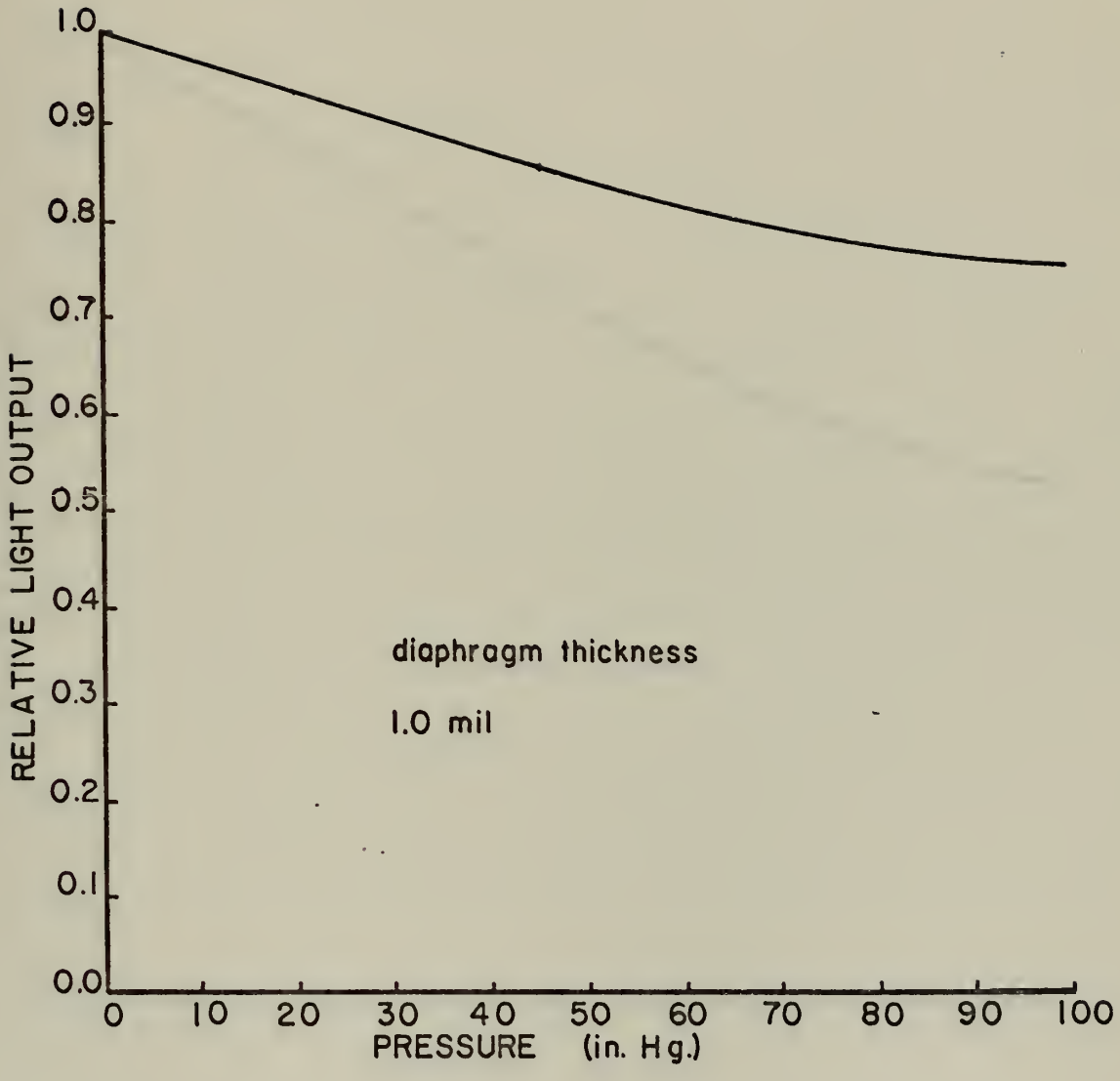

Figure 12. Light Output Versus Pressure Using a Laser Light Source.

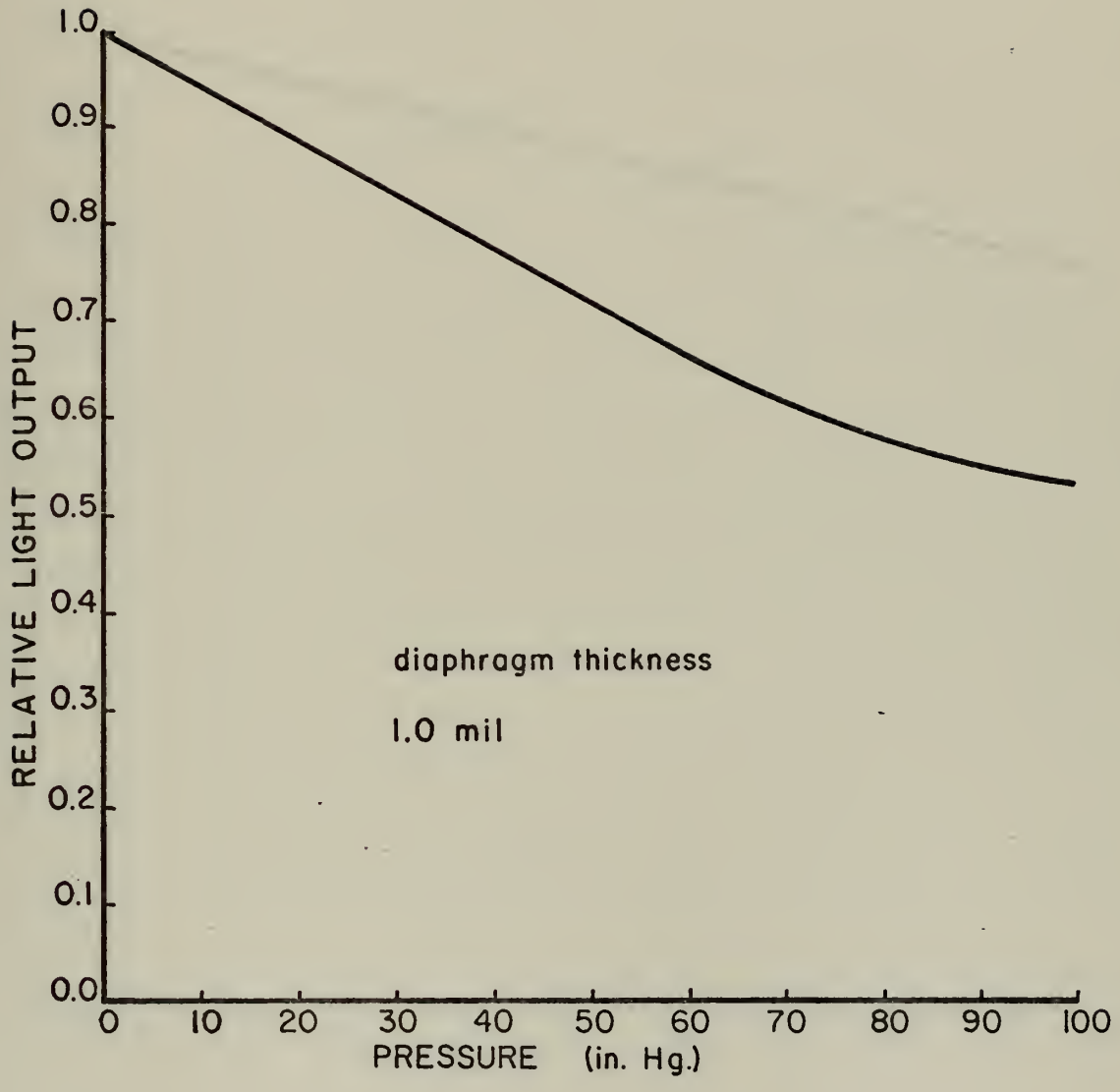

Figure 13. Light Output Versus Pressure for 0.125 Inch Diameter Transducer.

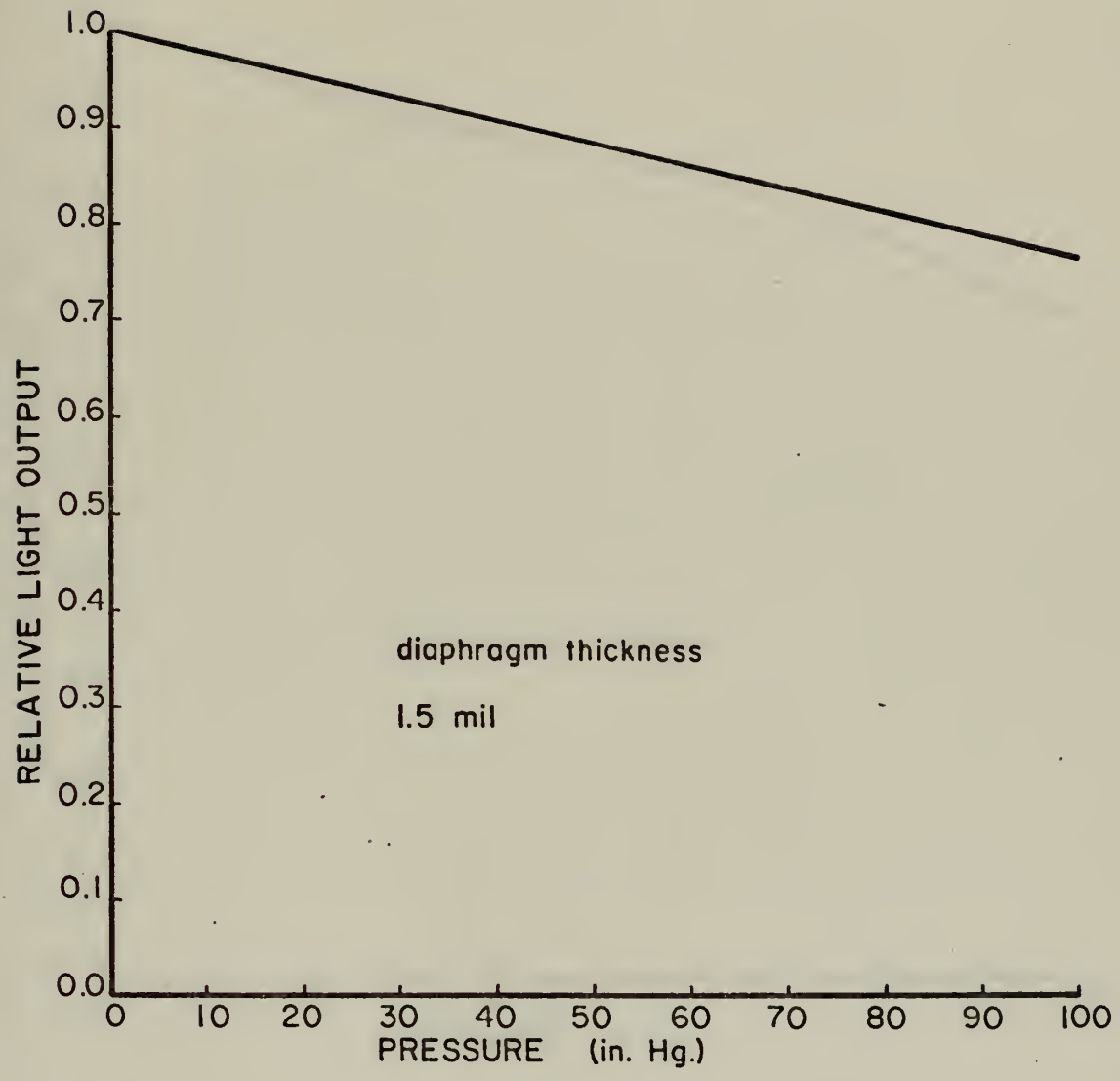

Figure 14. Light Output Versus Pressure for Near Side Probe Location.

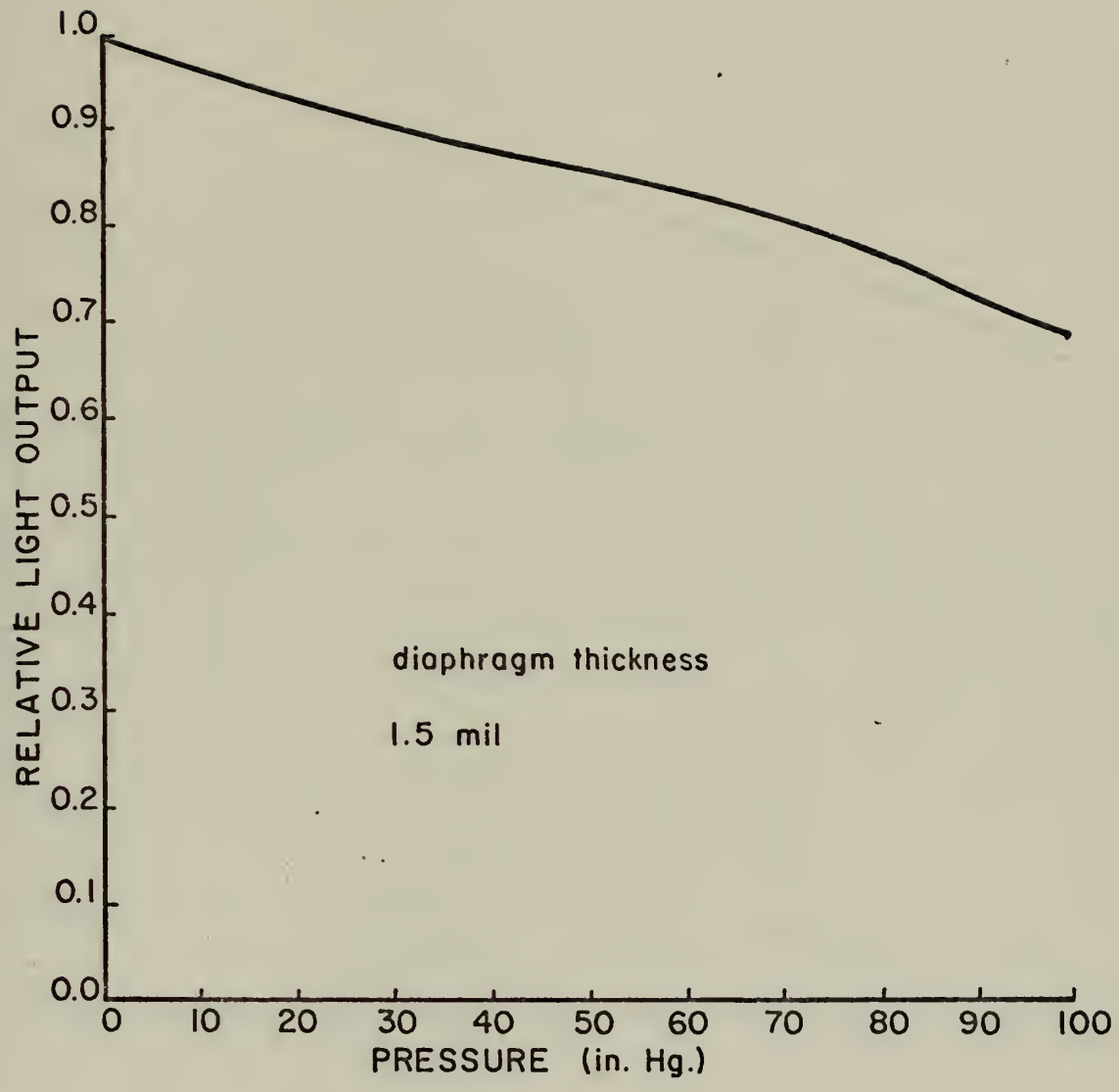

Figure 15. Light Output Versus Pressure for Peak Probe Location.

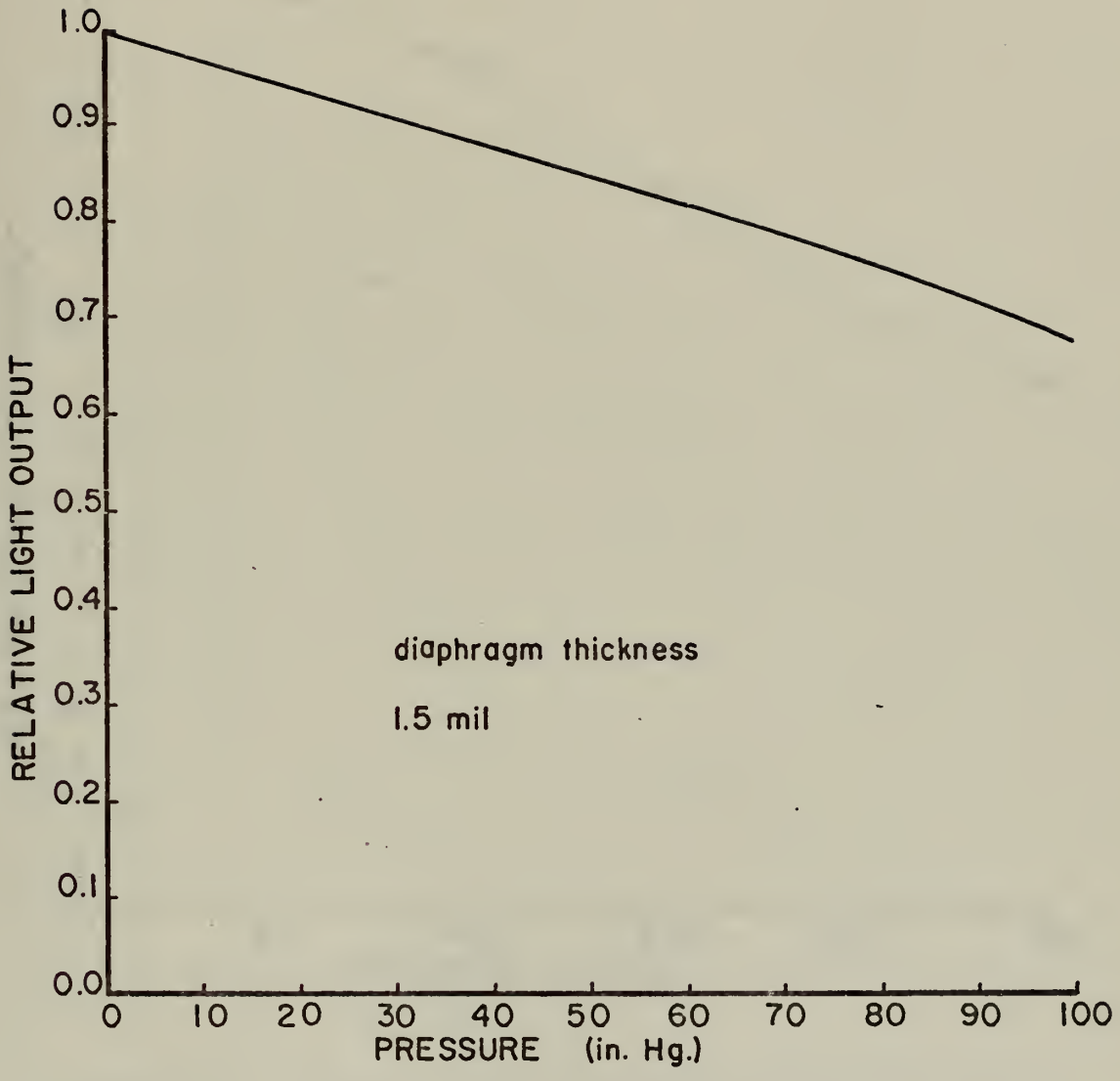

Figure 16. Light Output Versus Pressure for Far Side Probe Location.

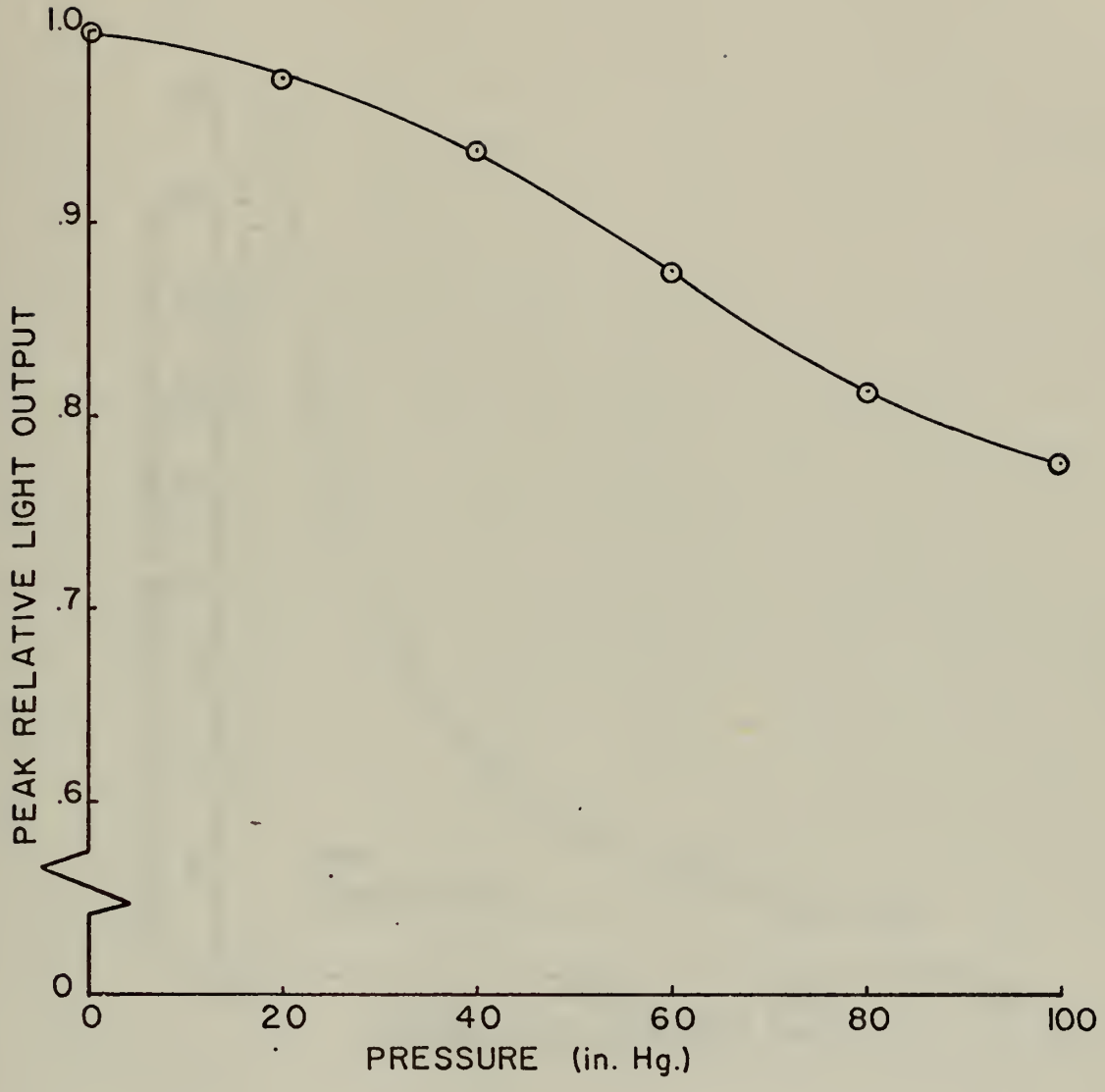

Figure 17. Effect of Pressurized Diaphragm on Peak Light Output.

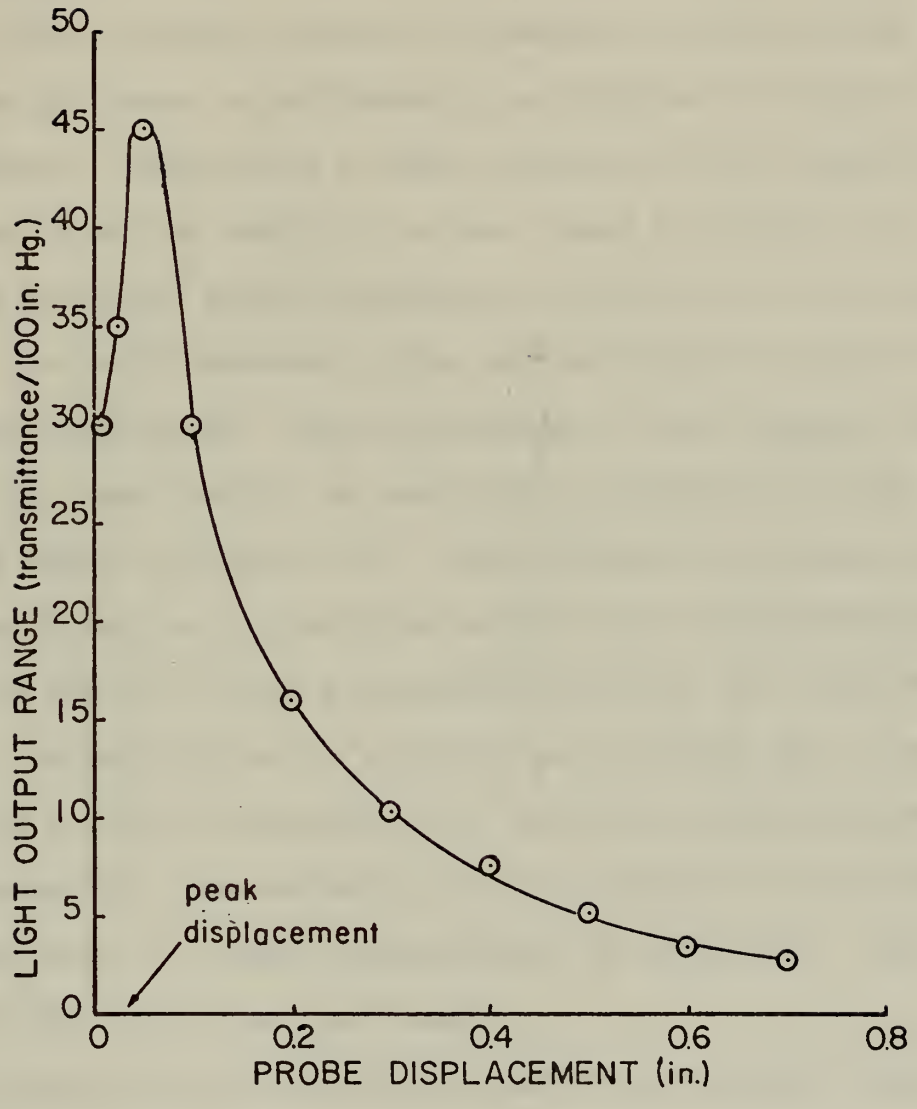

Figure 18. Effect of Probe Displacement on Light Output Range.

III. LASER DIGITAL PRESSURE TRANSDUCER

A. CONCEPT [Ref. 9,10]

The laser digital pressure transducer evolves from the principle of laser interferometry as applied to linear measurement. Reflecting a small portion of the output laser beam back into the cavity of a gas laser by means of a moveable external mirror produces a modulation in the laser power. For each movement of the mirror equal to one-half the radiation wavelength, the oscillation of the standing wave within the laser cavity is amplitude modulated through one cycle as shown in Figure 19. The modulated intensity of the laser beam can be detected easily by a photomultiplier tube. If the laser has a secondary beam at the rear of the cavity, the modulation is visible to the naked eye. By employing a digital apparatus to count the peaks in intensity produced by the external mirror movement, an extremely accurate means of linear measurement is afforded - equal to one-half the radiation wavelength.

The laser digital pressure transducer extends this principle to pressure measurement by integrating the moveable mirror with a pressure sensing diaphragm. Centerline deflection of the diaphragm-mirror combination is the displacement causing modulation. This proposed transducer has three major advantages, provided the deflection characteristics of the diaphragm are known:

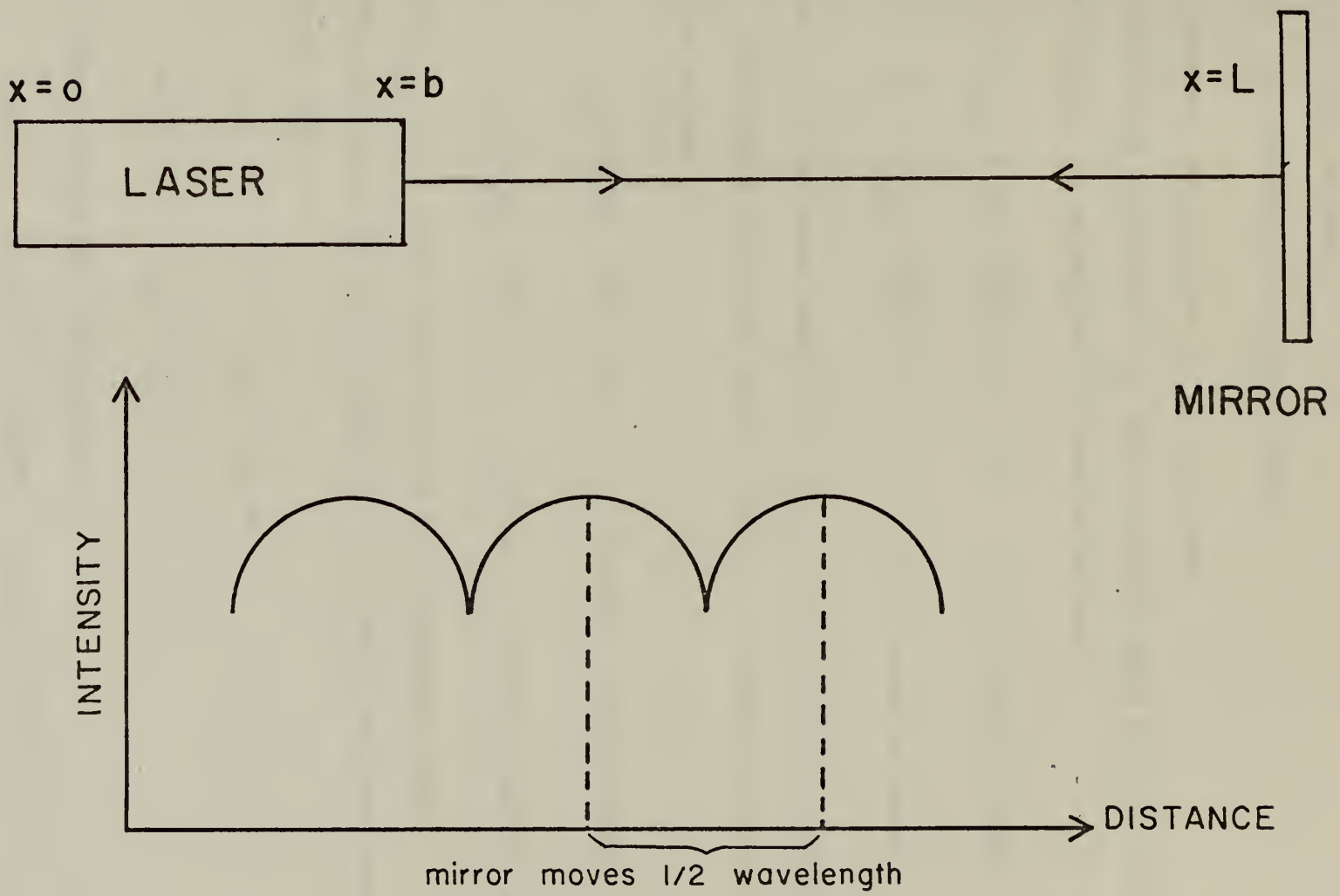

Figure 19. Intensity Peaks with Change in Optical Path.

1. Discrete, digital output
2. High accuracy
3. No calibration requirements

B. EXTERNAL MODULATION OF A GAS LASER

Referring to Figure 19, the standing wave within the laser cavity is described by two equations:

$$A_R = A_o \sin\left(\frac{2\pi x}{\lambda} - \omega t - \phi\right) \quad \text{(right running wave)}$$

$$A_L = A_o \sin\left(\frac{2\pi x}{\lambda} + \omega t + \phi\right) \quad \text{(left running wave)}$$

where A_o is the peak amplitude of the wave without modulation. The wave external to the cavity is described in a similar manner.

$$C_R = C_o \sin\left(\frac{2\pi x}{\lambda} - \omega t - \phi\right) \quad \text{(right running wave)}$$

$$C_L = C_o \sin\left(\frac{2\pi x}{\lambda} + \omega t - \frac{4\pi L}{\lambda} + \phi\right) \quad \text{(left running wave)}$$

where C_o is the peak amplitude of the external wave.

The electric field is zero at the cavity mirrors and the external mirror:

$$\text{at } x = 0, t = 0, \quad C_R + C_L = 0$$

$$\text{at } x = L, \quad A_R + A_L + C_R + C_L = 0 \ .$$

The latter condition determines ϕ:

$$A_o \sin\phi - A_o \sin\phi - C_o \sin\phi + C_o\left(\sin\phi - \frac{4\pi L}{\lambda}\right) = 0$$

$$\sin\phi + \sin\left(\phi - \frac{4\pi L}{\lambda}\right) = 0$$

$$\phi = \frac{2\pi L}{\lambda} \ .$$

Then

$$A_R = A_o \sin\left[\frac{2\pi}{\lambda}(x - L) - \omega t\right]$$

$$A_L = A_o \sin\left[\frac{2\pi}{\lambda}(x + L) + \omega t\right]$$

$$C_R = C_o \sin\left[\frac{2\pi}{\lambda}(x - L) - \omega t\right]$$

$$C_L = C_o \sin\left[\frac{2\pi}{\lambda}(x + L) + \omega t\right] .$$

Checking this result at x = b, the electric field intensity is found to be zero at the cavity mirror located at b.

$$A_R + A_L + C_R + C_L = A_o \sin\left(n\pi - \frac{2\pi L}{\lambda}\right) + A_o \sin\left(n\pi + \frac{2\pi L}{\lambda}\right) = 0$$

At $x = \lambda/4$ and $t = 0$, the amplitude is:

$$A_R + A_L + C_R + C_L = A_o\left[\sin\left(\frac{\pi}{2} - \frac{2\pi L}{\lambda}\right) + \sin\left(\frac{\pi}{2} + \frac{2\pi L}{\lambda}\right)\right]$$

$$+ C_o\left[\sin\left(\frac{\pi}{2} - \frac{2\pi L}{\lambda}\right) + \sin\left(\frac{\pi}{2} + \frac{2\pi L}{\lambda}\right)\right]$$

$$= (A_o + C_o)\left[\sin\left(\frac{\pi}{2} - \frac{2\pi L}{\lambda}\right) + \sin\left(\frac{\pi}{2} + \frac{2\pi L}{\lambda}\right)\right]$$

$$= (A_o + C_o)\left[\sin\frac{\pi}{2}\cos\left(\frac{-2\pi L}{\lambda}\right) - \sin\frac{2\pi L}{\lambda}\cos\frac{\pi}{2}\right.$$

$$\left. + \sin\frac{\pi}{2}\cos\frac{2\pi L}{\lambda} + \sin\frac{2\pi L}{\lambda}\cos\frac{\pi}{2}\right]$$

$$= 2(A_o + C_o)\cos\frac{2\pi L}{\lambda} .$$

With $L = (m + f)\lambda$, $\begin{cases} 0 \leq f < 1 \\ m \text{ an integer} \end{cases}$

the amplitude is:

$$A_R + A_L + C_R + C_L = 2(A_o + C_o)\left[\frac{\cos(m + f)2\pi\lambda}{\lambda}\right]$$

$$= 2(A_o + C_o)\ \cos 2\pi m \cos 2\pi f - \sin 2\pi m \sin 2\pi f$$

$$= 2(A_o + C_o)\ \cos 2\pi f\ .$$

With f corresponding to fractional wavelengths of mirror movement,

$f = 1/4$: $\cos \pi/2 = 0$

$f = 1/2$: $\cos \pi = -1$

$f = 3/4$: $\cos 3\pi/2 = 0$

$f = 1$: $\cos 2\pi = +1$.

Since intensity is proportional to the square of the wave amplitude,

$$\text{Intensity} \sim 4(A_o + C_o)^2 \cos^2 2\pi f;$$

and the intensity peaks are of the form illustrated in Figure 20:

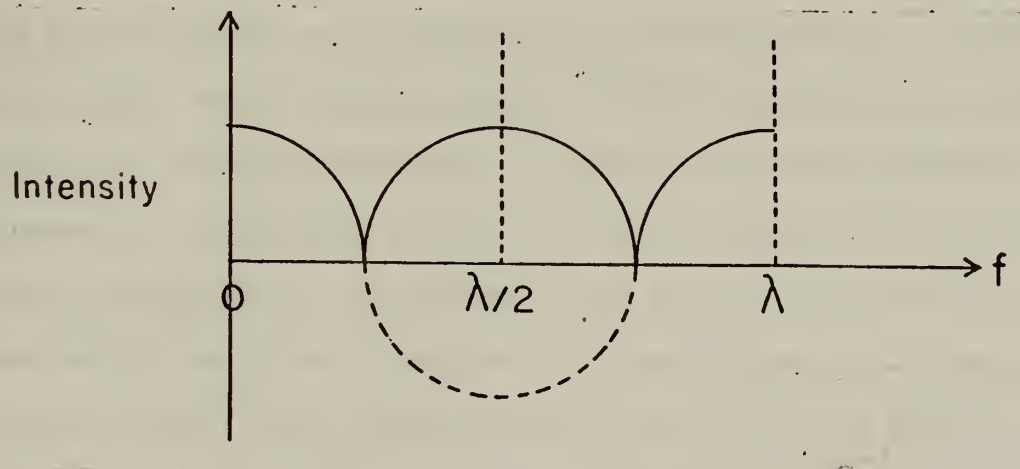

Figure 20. Laser Intensity Modulation.

The laser intensity undergoes one cycle of modulation with each complete wavelength change in optical path from the laser to the external mirror and back. Changes in the path length can be measured by counting maxima and minima in the laser intensity.

The He-Ne laser emits visible red light at 0.6328 micron wavelength and infrared at 3.391 microns wavelengths. This concept of linear measurement allows accuracy to within 0.3164 micron.

C. EXPERIMENTAL LASER MODULATION

Before attempting to build the laser digital pressure transducer, an experiment was performed to verify the modulation principle. A Hughes model 1708 He-Ne laser, rated at 1.0 milliwatt power, was chosen for this purpose, as this laser had, in addition to the primary beam, a secondary beam at the rear of the cavity which facilitated intensity measurement. The moveable external mirror was adapted from the plane mirror on a Michelson interferometer. The photomultiplier tube was positioned at the secondary beam and connected to the photometer. This arrangement appears in Figure 21. A geared knob on the interferometer permitted axial movements of the mirror that were approximately one wavelength per turn. The mirror was aligned such that the primary laser beam was reflected back into the cavity.

As the mirror was moved toward the laser cavity, intensity modulation was observed in both the secondary laser beam and the photometer indicator. The output indicator

varied smoothly between maximum and minimum values corresponding to mirror movement. In achieving the modulation effect, the mirror alignment was found to be very sensitive, and a moderate amount of adjustment was necessary before the desired results were attained.

D. TRANSDUCER DESIGN AND EXPERIMENTAL ARRANGEMENT

From the successful results obtained in the modulation experiment, a prototype laser digital pressure transducer was built. A 1.8-inch diameter, spherical, gold coated mirror (focal length: 25 centimeters) was secured in a circular frame, which in turn was fastened to a brass diaphragm (thickness: 25 mils; diameter: 2 inches) by a small amount of solder at the frame center. This diaphragm-mirror combination was clamped at the edge of a 2-inch inner diameter pressure chamber by an O-ring and collar arrangement to form the transducer.

The experimental arrangement is shown in Figure 22. Pressure to the transducer was supplied from the Lockheed test rig. The transducer was positioned such that the beam from the Hughes model 1710 laser was reflected from the mirror back into the cavity.

E. EXPERIMENTAL RESULTS AND DISCUSSION

As pressure was applied to the transducer diaphragm, intensity modulation was observed on the photometer output indicator, although not of the form observed in the modulation experiment. The characteristic photometer indication

consisted of a marked modulation in the initial pressure application, followed by a stabilized response with further pressure application above about 5.0 inches Hg., as shown in Figure 23. The degree and range of modulation as observed on the photometer output indicator varied with each separate mirror realignment. It became apparent after several attempts that proper mirror alignment was not possible due to nonuniformities in the diaphragm-mirror interface. Since the mirror was not joined to the exact center of the diaphragm, deflections of the latter produced mirror movements that were more pivotal than axial. The observed modulation in this case was caused by the reflected beam moving across the laser cavity window. Stabilized response occurred as the beam moved out of the cavity window.

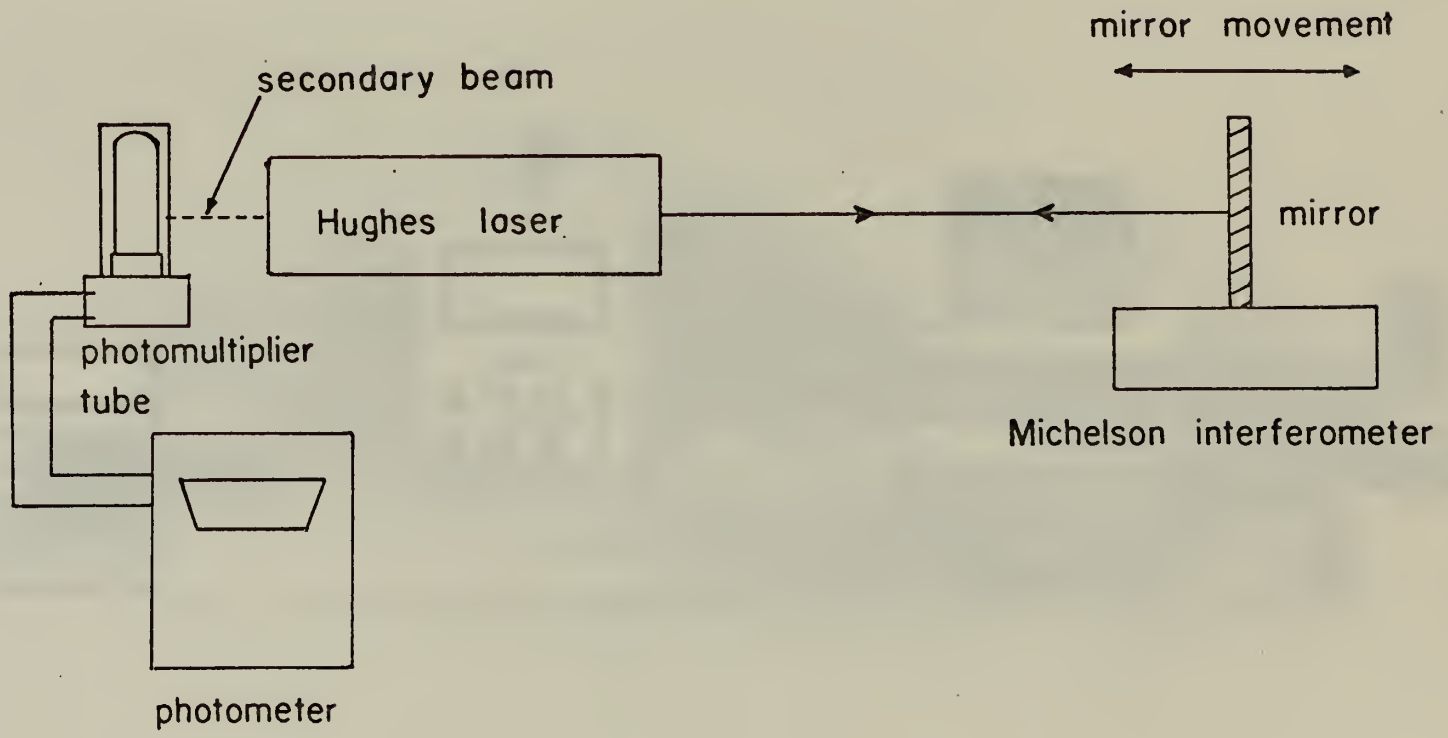

Figure 21. Arrangement for Laser Modulation Experiment.

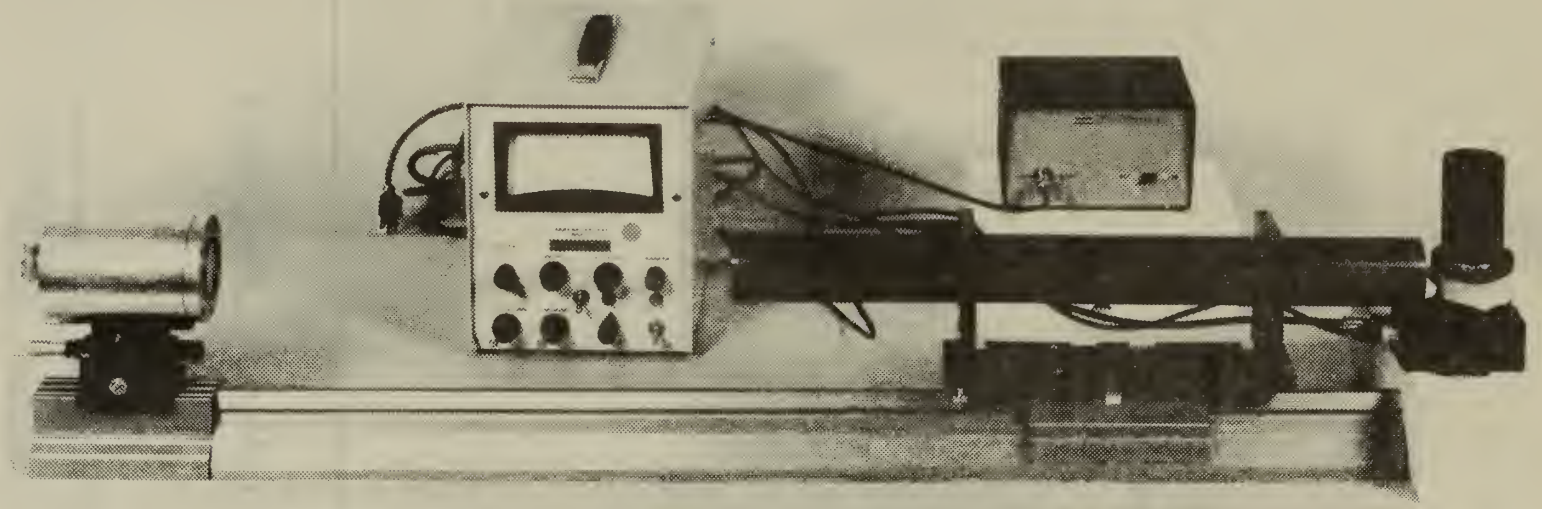

Figure 22. Arrangement for Test of Laser Digital Pressure Transducer. From left; transducer in mount; photometer, Hughes 1710 laser; laser power supply; and photomultiplier tube.

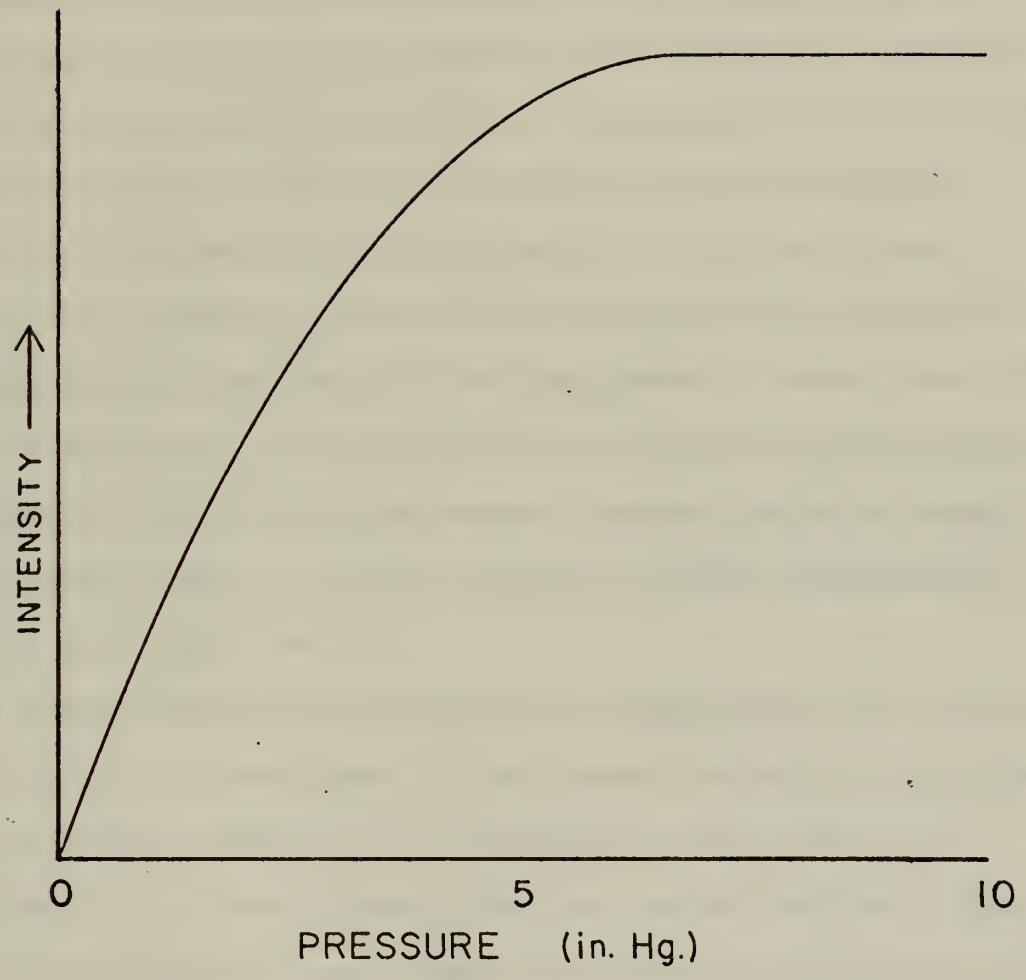

Figure 23. Response of Laser Digital Pressure Transducer.

IV. CONCLUSIONS AND RECOMMENDATIONS

Linearity of the fiber optic pressure transducer response is dependent on the amount of diaphragm deflection. A transition to non-linear response occurs as the deflection approaches the diaphragm thickness. Curvature of the diaphragm is the dominant factor in the response, causing a decrease in light output with increasing pressure for all probe locations. The probe location and the diaphragm deflection determine the sensitivity. For the probes tested, the greatest sensitivity occurred with the probe located on the far side of the displacement curve, near the peak of the curve. The sensitivity decreases as the range of diaphragm deflection decreases, necessitating a compromise between sensitivity and range of linear response for a particular application.

A better method of mounting the diaphragm to the transducer should be developed. The present soldering technique limits further reduction in transducer size due to non-uniformities in the solder joint and contamination of the inner diaphragm surface. Some consideration should be given to different fiber bundle distributions in the probe. Previous research [Ref. 7] employed random and split fiber bundle distributions, with little difference observed in response other than sensitivity. With the diaphragm curvature governing the overall response, probes employing the

latter two distributions would be easier and less costly to manufacture. Temperature effects and frequency response need to be investigated. The temperature effects can be determined only when a better method of mounting the transducer is found, as the presently used solder would melt at higher temperatures.

Intensity modulation of a gas laser is possible by reflecting a portion of the laser beam back into the cavity by use of an external moveable mirror. Intensity maxima and minima were experimentally observed for pure axial movements of the mirror corresponding to half-wavelengths of laser radiation. Alignment of the laser and mirror axes is critical. Adaptation of this principle to pressure measurement was not achieved due to alignment problems. Based on the success with the modulation experiment, it is evident the technique will work when alignment problems are solved.

APPENDIX A

ANALYSIS OF DIAPHRAGM DEFLECTION AND CURVATURE

The diaphragm is treated as a flat, circular plate with clamped edges. Flat plate theory assumes a neutral middle plane. In a cubical element of the plate subjected to bending, the vertical planes remain plane and perpendicular to the horizontal neutral plane. Any strain in the middle neutral plane can be neglected during bending. For the analysis to be valid, the deflection of the diaphragm must be small compared to the radius and thickness. For deflections greater than one-half the thickness, a transition to membrane theory is necessary.

The following assumptions are made:

1. The diaphragm is flat and homogeneous
2. The thickness is less than one-quarter of the radius and is at least twice the maximum deflection.
3. The load is distributed equally, normal to the free surface of the diaphragm.

From the clamped edge condition, two boundary conditions arise: the deflection along the edge is zero and the tangent plane to the deflected middle surface along the edge coincides with the initial position of the middle plane of the diaphragm:

$$x)_{r=a} = 0 \ , \qquad \frac{\partial x}{\partial r}\Big)_{r=a} = 0 \ .$$

At the origin, the slope is zero:

$$\frac{\partial x}{\partial r}\Big)_{r=0} = 0 \ .$$

As the diaphragm is deflected, one surface of the diaphragm is subject to compression and the other surface is subjected to tension. Compression of an elastic material causes an expansion in the direction normal to the force. The degree of expansion is given by Poisson's ratio, ν.

An equation for the deflection of a uniformly loaded, flat plate (diaphragm) with clamped edges is [Ref. 8]:

$$x = \frac{3p(1-\nu^2)(a^2-r^2)^2}{16Et^3} \ . \qquad \text{(A-1)}$$

Maximum deflection of the diaphragm is at r = 0:

$$x_{max} = \frac{3p(1-\nu^2)a^4}{16Et^3} \ . \qquad \text{(A-2)}$$

The slope of the diaphragm at a radius, r, is:

$$\frac{\partial x}{\partial r} = \frac{-3pr(1-\nu^2)(a^2-r^2)}{4Et^3} \ . \qquad \text{(A-3)}$$

APPENDIX B

WALL REFLECTION EFFECTS

The characteristic displacement curve is altered somewhat by the effects of a reflecting wall surrounding the probe and working (reflecting) surface. The qualitative effect is best visualized in a 2-dimensional graphical analysis. Assumptions used in this analysis are:

1. As in Appendix C, the emergent angle of an individual light ray is assumed to be a function of radial distance from the probe axis, i.e., at the axis, the emergent angle is zero, and at r_o the emergent angle is equal to the half-angle of the emergent light cone.

2. Wall reflectivity is equal to the reflectivity of the primary reflecting surface.

Emergent light rays from the inner fiber bundle can be described in one of three categories, illustrated below:

1. Primary reflected ray: The emergent ray is reflected directly from the primary reflecting surface to the outer fiber bundle, as shown in Figure 24.

2. Secondary reflected ray: The emergent ray is reflected from the primary reflecting surface to the wall, and from the wall to the outer fiber bundle; see Figure 25.

3. Wall terminated ray: The emergent ray is reflected from the wall to the primary reflecting surface, and then to a point other than on the outer fiber bundle; refer to Figure 26.

Only the first two categories of emergent rays influence the light output on the displacement curve. For a given displacement of the probe from the primary reflecting surface, the range of emergent rays in a category can be graphically determined. For primary reflected rays, the radial distance between the outermost and innermost rays, Δr, is measured, as are their respective emergent angles, θ_1 and θ_2. From Figure 3, the relative intensities of the two rays are weighted according to their emergent angles.

Multiplying Δr by the average intensity of the outermost and innermost rays gives a qualitative approximation of the light output from primary reflected rays. The same procedure is followed for the category of secondary reflected rays. Adding the light output calculated from secondary reflected rays to that from primary reflected rays provides a measure of wall reflection effects.

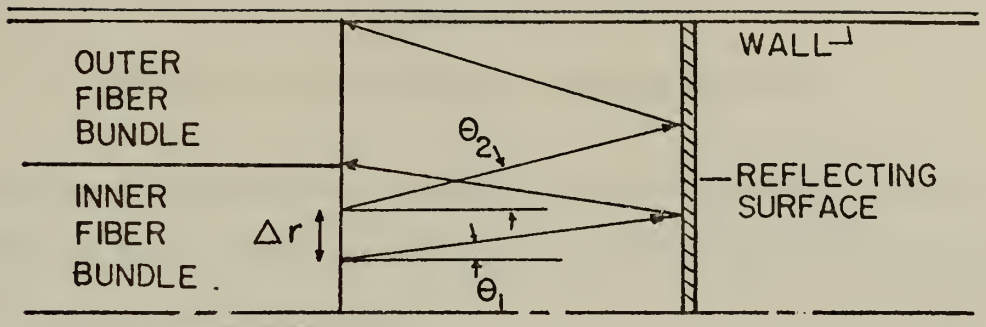

Figure 24. Primary Reflected Rays.

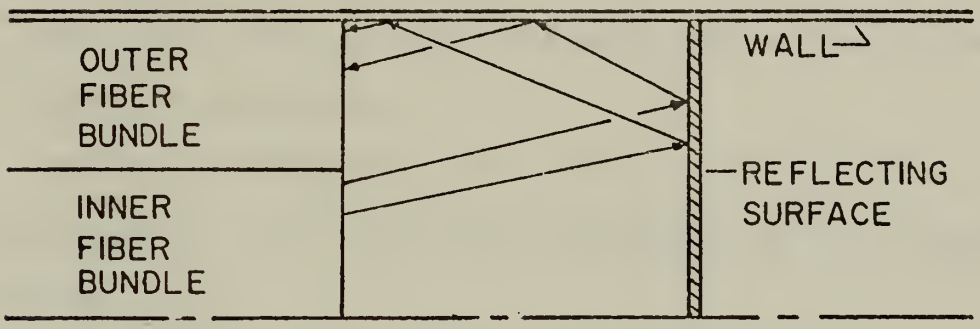

Figure 25. Secondary Reflected Rays.

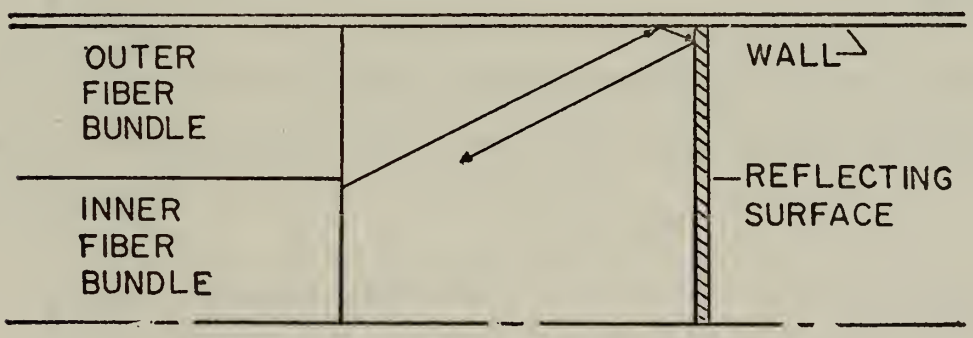

Figure 26. Wall Terminated Rays.

APPENDIX C

GEOMETRIC ANALYSIS OF OPTICAL COUPLING

For the 2-dimensional geometric analysis that follows, the case of a pressurized diaphragm will first be considered. Three assumptions are made:

1. θ, the emergent angle of an individual light ray, varies uniformly over the inner fiber bundle radius, from 0 degrees to θ_R, the half-angle of the emergent light cone of the fiber bundle, i.e., $\theta = \theta(r)$.
2. The probe face is flat and parallel to the unpressurized diaphragm.
3. Wall reflection does not occur.

From Equation A-1, the axial deflection of the diaphragm at a radius, R, is:

$$x = \frac{3p(1-\nu^2)(a^2 - R^2)^2}{16Et^3} \quad . \qquad \text{(C-1)}$$

The axial distance, X, from R to the probe face is:

$$X = D - x \quad , \qquad \text{(C-2)}$$

where D is the initial probe displacement relative to the diaphragm. Combining (C-1) and (C-2), and grouping constants into K_1 yields

$$X = D - K_1(A^2 - R^2)^2 \quad . \qquad \text{(C-3)}$$

A light ray emerging from the inner fiber bundle at a radius r and angle θ intercepts the diaphragm at R. R is then a function of r, θ, and X:

$$R = (\tan \theta)X + r \quad , \tag{C-4}$$

The relation can be seen more clearly by recalling the familiar equation for a straight line, $y = mx + b$, with $\tan \theta = m$, $X = x$, $r = b$, and $R = y$.

Equations (C-3) and (C-4) can be solved for R and X. Solving for R,

$$R = (\tan \theta)(D - K_1(a^2 - R^2)^2) + r \quad . \tag{C-5}$$

Expanding,

$$K_1R^4\tan\theta - 2K_1a^2R^2\tan\theta - R = -D\tan\theta + K_1a^4\tan\theta + r \quad .$$

This lengthy result can be simplified by setting $K_2 = K_1\tan\theta$ and noting that the right side is constant for an individual ray:

$$K_2R^4 - (2K_2a^4)R^2 - R = K_3 \quad . \tag{C-6}$$

Solution of (C-6) yields R, the intercept of the light ray and the diaphragm.

The value of X at R is found from (C-4). The slope of the curved diaphragm at R is, from (A-3),

$$x'_{\cdot} = \frac{-3pR(1 - \nu^2)(a^2 - R^2)}{4Et^3} \quad .$$

After reflection from R on the diaphragm, the light ray intercepts the probe face at Y:

$$Y = X(\tan(\theta + 2\tan^{-1}(x')) + X\tan\theta + r \quad .$$

From this result, two values of r can be found by iteration: r_1, for which Y is equal to the inner radius of the outer fiber bundle, and r_2, for which Y is equal to the outer radius of the outer fiber bundle. The limiting radii, r_1 and r_2 are referred to in the optical coupling theory of Section H.

The analysis is simplified when considering the case of a flat reflecting surface. In this case, the deflection and curvature of the diaphragm are zero and the displacement of the probe is the variable. Then,

$$X = D - 0$$

$$= D \quad ,$$

and,

$$Y = 2D\tan\theta + r \quad .$$

LIST OF REFERENCES

1. Siegmund, W. P., and others, Applied Optics and Optical Engineering, v. 4, part 1, p. 1-13.

2. Potter, R. J., "Transmission Properties of Optical Fibers," J. Opt. Soc. Am., v. 51, n. 10, p. 1079-1089, October, 1961.

3. St. Clair, J., "Fiber Optics: Theory and Applications," Bendix Technical Journal, p. 67-76, Summer, 1969.

4. Morita, E., and Takase, M., "Angular Distribution of Light Emitted from the Optical Fiber Bundle," Japan J. Appl. Phys., v. 6, p. 414-415, 1967.

5. Kapany, N. S., "Fiber Optics. V. Light Leakage due to Frustrated Total Reflection," J. Opt. Soc. Am., v. 49, n. 8, p. 771-777, August, 1959.

6. Mechanical Technology Inc., Specifications Sheet, "KD-100 Fotonic Sensor," Personal correspondence.

7. Margerum, G. W., "A Fiber Optic Pressure Transducer," Ae. E. Thesis, Naval Postgraduate School, Monterey, California, June 1972.

8. Timoshenko, S., "Theory of Plates and Shells," p. 54-55, 83, McGraw-Hill, 1959.

9. Ashby, D. E. T. F., Jephcott, D. F., Malein, A., Raynor, F. A., "Performance of the He-Ne Gas Laser as an Interferometer for Measuring Plasma Density," J. Appl. Phys., v. 36, n. 1, p. 29-30, January, 1965.

10. Ashby, D. E. T. F., Jephcott, D. F., "Measurement of Plasma Density Using a Gas Laser as an Infrared Interferometer," Appl. Phys. Letters, v. 3, n. 13, 1963.

INITIAL DISTRIBUTION LIST

		No. Copies
1.	Defense Documentation Center Cameron Station Alexandria, Virginia 22314	2
2.	Library (Code 0212) Naval Postgraduate School Monterey, California 93940	2
3.	Chairman, Department of Aeronautics (Code 57) Naval Postgraduate School Monterey, California 93940	1
4.	Professor A. F. Fuhs, Code 57Fu Department of Aeronautics Naval Postgraduate School Monterey, California 93940	5
5.	Professor R. P. Shreeve, Code 57Sf Department of Aeronautics Naval Postgraduate School Monterey, California 93940	1
6.	LT J. W. Leonard Code 31 Naval Postgraduate School Monterey, California 93940	1
7.	Mr. Karl Guttmann, Code 330 Naval Air Systems Command Washington, D.C. 20360	1
8.	Mr. Irv Silver, Code 03 Naval Air Systems Command Washington, D.C. 20360	1
9.	Dr. Frank Tanczos, Code 03 Naval Air Systems Command Washington, D.C. 20360	1
10.	Mr. Eric Lister Research and Technology Naval Air Propulsion Test Center Trenton, New Jersey 08628	1

11. Mr. Albert Martino 1
Research and Technology
Naval Air Propulsion Test Center
Trenton, New Jersey 08628

12. Mr. Albert G. Powers 1
NASA Lewis Research Center
Cleveland, Ohio 44135

13. Mr. Joseph Batka 1
AFAPL/TBC
Wright-Patterson AFB, Ohio 45433

14. Mr. Harry Snowball 1
AFFDL
Wright-Patterson AFB, Ohio 45433

15. Dr. Hans Von Ohain 1
Chief Scientist
ARL
Wright-Patterson AFB, Ohio 45433

16. Mr. Terry Trumble 1
AFAPL
Wright-Patterson AFB, Ohio 45433

17. Mr. Robert A. Langworthy 1
Eustis Directorate
SAVDL-EV-PP
USAAMRDL
Fort Eustis, Virginia 23604

18. Dr. Gilbert Hollingsworth 1
Technical Director
Naval Air Development Center
Warminster, Pa. 18974

19. LCDR Gordon W. Margerum 1
Code 73
COMFAIR Hawaii
FPO San Francisco, California 96610

UNCLASSIFIED
Security Classification

DOCUMENT CONTROL DATA - R & D

(Security classification of title, body of abstract and indexing annotation must be entered when the overall report is classified)

1. ORIGINATING ACTIVITY (Corporate author)

Naval Postgraduate School
Monterey, California 93940

2a. REPORT SECURITY CLASSIFICATION

Unclassified

2b. GROUP

3. REPORT TITLE

FIBER OPTIC AND LASER DIGITAL PRESSURE TRANSDUCERS

4. DESCRIPTIVE NOTES (Type of report and inclusive dates)

Master's Thesis; June 1973

5. AUTHOR(S) (First name, middle initial, last name)

John W. Leonard; Lieutenant, United States Navy

6. REPORT DATE	7a. TOTAL NO. OF PAGES	7b. NO. OF REFS
June 1973	75	10

8a. CONTRACT OR GRANT NO.	9a. ORIGINATOR'S REPORT NUMBER(S)
b. PROJECT NO.	
c.	9b. OTHER REPORT NO(S) (Any other numbers that may be assigned this report)
d.	

10. DISTRIBUTION STATEMENT

Approved for public release; distribution unlimited.

11. SUPPLEMENTARY NOTES	12. SPONSORING MILITARY ACTIVITY

13. ABSTRACT

The theory and response of fiber optic pressure transducers were investigated in a continuation of previous research. A 0.125-inch diameter transducer was built and statically tested. A probe consisting of two concentric glass fiber bundles was used to transmit light to and from the transducer diaphragm. Response was linear through 60 inches Hg. Linearity and sensitivity of response were dependent on diaphragm thickness and probe location, respectively. In a separate experiment, a gas laser was externally modulated by means of a moveable mirror. Axial movement of the mirror corresponding to half-wavelengths of laser radiation produced intensity maxima and minima. This modulation concept was extended to pressure measurement by attaching the mirror to a pressure sensing diaphragm.

DD FORM 1 NOV 68 1473 (PAGE 1)
S/N 0101-807-6811

UNCLASSIFIED
Security Classification

A-31408

KEY WORDS	LINK A		LINK B		LINK C	
	ROLE	WT	ROLE	WT	ROLE	WT
FIBER OPTICS						
PRESSURE TRANSDUCER						
FIBER OPTIC PRESSURE TRANSDUCER						
LASER MODULATION						
DIGITAL PRESSURE TRANSDUCER						